This project has received funding from the European Union's Horizon Europe Programme

RESEARCH PROJECT EASA.2022.C25

D-2.1 REPORT ON MAIN INVESTIGATIONS PERFORMED AND USE CASES

MODEL-SI

Digital Transformation - Case Studies for Aviation Safety Standards - Modelling and Simulation

An Agency of the European Union

Disclaimer

Funded by the European Union. Views and opinions expressed are however those of the author(s) only and do not necessarily reflect those of the European Union or the European Union Aviation Safety Agency (EASA). Neither the European Union nor EASA can be held responsible for them.

DELIVERABLE NUMBER AND TITLE: [MODEL-SI, D-2.1 Report on main investigations performed and uses cases
CONTRACT NUMBER: EASA.2022.C25
CONTRACTOR / AUTHOR: ZHAW / Marcello Righi
IPR OWNER: European Union Aviation Safety Agency
DISTRIBUTION: Public

REV #	DATE	AUTHORS	REVIEWER
1	13.10.2024	Andrea Pedrioli, Andrea Vaiuso, Noé Pedrazzini, Marcello Righi, Xinying Liu, Oier Coretti, Moreno Apicella	Marcello Righi

DATE: 13 October 2024

SUMMARY

The continual advancements in Artificial Intelligence (AI) and in particular in Machine Learning (ML) have the potential to revolutionize the design and development processes for Vertical Take-Off and Landing (VTOL) vehicles and drones. However, in order to grasp these methods, changes in certification and aviation standards are needed. To explore which methods and techniques are effectively valid, a case study in the development of a data-driven Digital Twin (DT) is presented. The methods used and described in this deliverable are based on our previous literature review [1].

The DT has been built upon a classical physics-based mathematical model. This model has been enhanced in terms of both accuracy and scope by leveraging data from various sources: high-fidelity (HF) numerical simulations (including Computational Fluid Dynamics (CFD) and structural dynamics) and flight tests. Both conventional and ML techniques were employed strategically to achieve optimal results. Thanks to data fusion techniques, the DT is able to combine the necessary accuracy provided by the initial physics-based model with the additional capabilities of several surrogate models. The final result could accurately predict the entire flight envelope and load distributions. In addition, to assess the trustworthiness of the DT prediction, a method which provides the epistemic uncertainties is chosen. Thanks to the probabilistic approach introduced with Bayesian Neural Networks (BNN), we can evaluate the uncertainties and therefore be empowered to make informed decisions based on the confidence outcome.

CONTENTS

ABBREVIATIONS

ACRONYM	DESCRIPTION
AI	Artificial Intelligence
ANN	Artificial Neural Networks
AOA	Angle of Attack
AOS	Angle of Sideslip
AP	Airplane
BEM	BEM Blade Element Momentum
BNN	Bayesian Neural Networks
CFD	Computational Fluid Dynamics
DDES	Delayed Detached Eddy Simulation
DoF	Degree of Freedom
DF	Data Fusion
DMD	Dynamic Mode Decomposition
DNN	Deep Neural Network
DT	Digital Twin
EASA	European Union Aviation Safety Agency
eVTOL	Electrical Vertical Take-Off and Landing
FCS	Flight Control System
FEM	Finite Element Method
FFT	Fast Fourier Transform
FSM	Flight Simulation Model
FT	Flight Test
HC	Helicopter
HF	High-Fidelity
GP	Gaussian process
LED	Large Eddy Simulation
LF	Low-Fidelity
LHS	Latin Hypercube Sampling
LL	Lifting Line
MF	Mid-Fidelity
ML	Machine Learning
NL	Non Linear
NN	Neural Networks
NS	Navier-Stokes
PID	Proportional-Derivative-Integral
POD	Proper Orthogonal Decomposition
RANS	Reynolds-averaged Navier–Stokes
ROM	Reduced Order Model

RPM	Round per Minute
SA	Spalart-Allmaras
SP	Surface Panel
SST	Shear Stress Transport
TL	Transfer Learning
VLM	Vortex Lattice Method
VPM	Vortex Particle Method
VTOL	Vertical Take-Off and Landing
UAV	Unmanned Aerial Vehicle
UQ	Uncertainty Quantification

1. Introduction and coding strategy

The following section introduces the methodology and implementation strategy followed during the case study.

1.1 Digital Twin

A digital twin (DT) is a virtual representation of a physical object, system, or process that is designed to accurately replicate its real-world counterpart in real-time. This digital replica utilizes data from sensors and other sources to mirror the physical entity's behaviour, conditions, and performance. By integrating data analytics, machine learning, and simulation, DTs enable monitoring, diagnostics, optimization, and predictive maintenance of the physical entity, thereby improving decision-making and operational efficiency.

1.1.1 Analysis of Digital Twin Data and Decision Making

It goes without saying that the availability of a DT makes the generation of large quantities of data possible. For instance, it is envisageable to carry out large quantities of simulations in time domain, in which different types of gusts and different configurations are used.

Parameters Space

Which parameters must be considered when generating this type of data is probably a decision the Authorities must make as the resulting parameters space must match the certification basis (i.e. which types of excitation must be considered, which flight envelope, which configurations).

Objectives / Costs Functions

In order to evaluate the data generated, a number of functions must be identified, which allow quantifying the safety margin of the drone. The identification of such functions would assist in compliance demonstration.

Methodologies (Clustering)

A number of different approaches are available. So far, we have only experimented with a clustering approach. In a limited example, we have generated a few thousand datasets, each one being a few seconds worth of signals, obtained from time simulations with different discrete wind gusts. The most relevant parameters are the gust intensity and its duration, the most meaningful indicators are bending and torsional moments at wing root. Figure 1 shows the results of clustering with 20 clusters. Each parameter is described as follows:

- ngusts : number of longitudinal discrete gusts
- dgust_max_length: max length of the discrete gusts
- gust_max_height: max intensity of the discrete gusts
- nlatgusts: number of lateral discrete gusts
- dlatgusts:max_height: max intensity of lateral gusts
- mb_norm: amplitude of bending moment
- mt_norm: amplitude of torsional moment

We selected the variable ranges for them to be plausible and chose a number of bands such that the solution was numerically consistent; shown here is the results for seven bands. In spite of this being an overly simplified example, the approach allows the identification of clusters of data, where the safety margins may be smaller,

and allows the identification of the related regions in the parameters space; in this case, being particularly easy to recognize that gusts with larger intensity and shorter durations are those more heavily impacting the structure.

Further Analysis of critical Areas on Parameters Space

It would be envisageable to build an AI model able to analyse the results of the clustering effort and make decisions (or provide the necessary information) as to which additional simulations (or flight tests) could be planned. Interestingly, the job of such a system would be to identify all relevant weaknesses in the system.

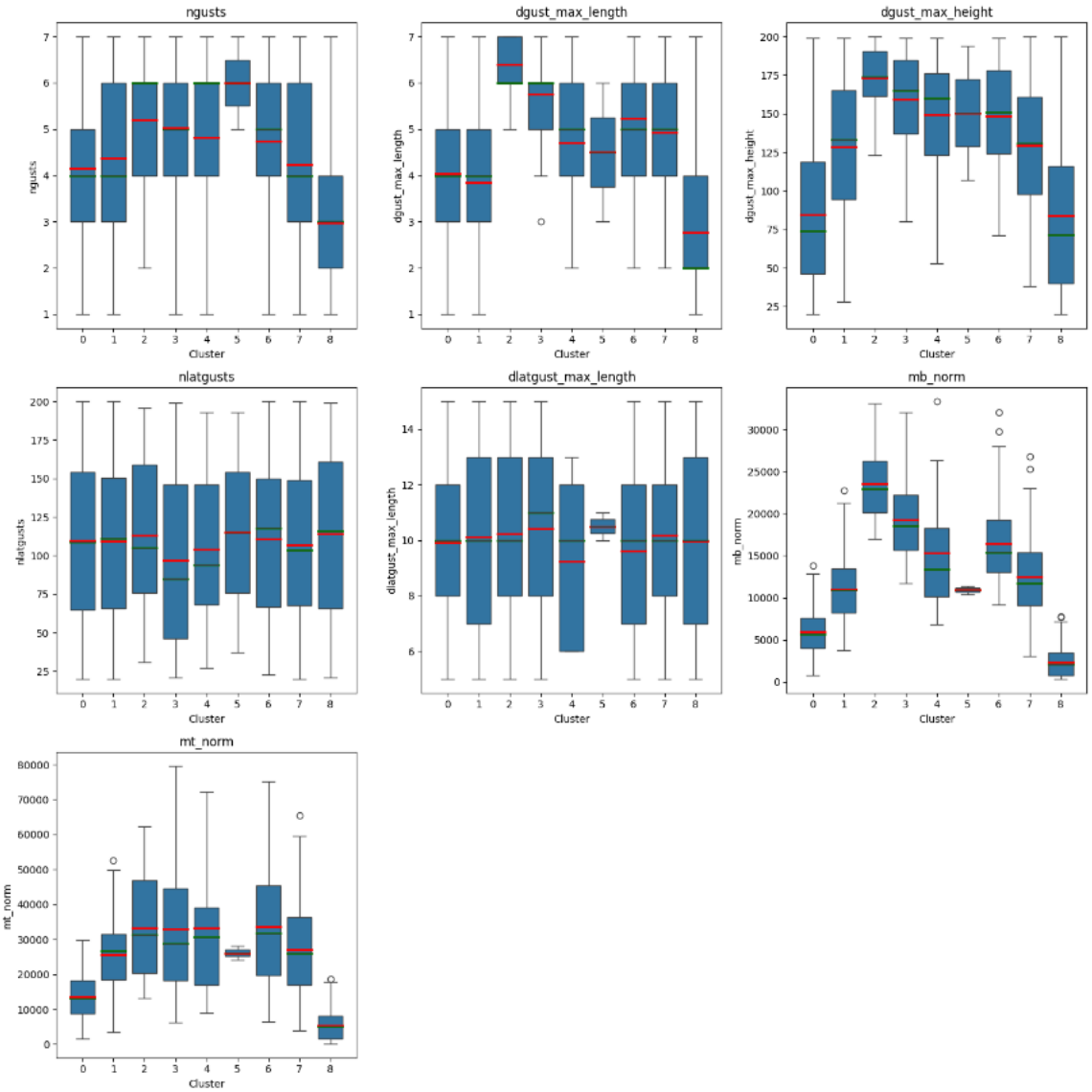

Figure 1: Bar charts showing the results of clustering a few thousand datasets, using bending and torsional moments at the wing root (ngusts : number of longitudinal discrete gusts, dgust_max_length: max length of the discrete gusts, gust_max_height: max intensity of the discrete gusts, nlatgusts: number of lateral discrete gusts, dlatgusts:max_height: max intensity of lateral gusts, mb_norm: amplitude of bending moment, mt_norm: amplitude of torsional moment).

1.2 Modular approach and its relevance

A modular approach is a design and development strategy that breaks down a system into distinct, self-contained units or modules, each with its own specific functions and interfaces. These modules can be independently developed, tested, and maintained before being integrated into the larger system. This approach enhances flexibility, scalability, and reusability, making complex systems easier to manage and adapt over time.
Modular approaches are therefore practical solutions when multiple disciplines are involved. A notable example is the method proposed by Prof. Karpel [2,3], provocatively named "increased order modelling." This approach, which has also been applied to certification and qualification purposes, progressively enhances the accuracy and physical fidelity of a linear aeroelastic kernel by incorporating additional modules. These modules can be used to account for aerodynamic nonlinearity, among other factors.

1.3 Modules

Our approach includes the following modules:

- A multi-fidelity surrogate model designed to predict rotor and wing forces based on the drone's speed, angle of attack, angle of sideslip, and rotors angular velocity.
- A MATLAB-SIMULINK-based flight mechanics solver, capable of trimming the drone and following a specified flight trajectory, with the addition of the lowest elastic modes.
- An aeroelastic solver that includes a Finite Element Model (FEM) wing model, the most relevant rigid body modes, and an elastic model of the rotors.

1.3.1 Flight Mechanics

Flight mechanics is the study of the forces and movements affecting an aircraft during flight. It involves examining the performance, stability, and control of aircraft to understand their behaviour under various conditions. This field integrates principles from aerodynamics, propulsion, structural dynamics, and control theory to ensure the safe and efficient operation of aircraft.

1.3.2 Aeroelasticity

Aeroelasticity encompasses an interdisciplinary study focusing on the interaction between aerodynamic forces and structural dynamics within flexible aerospace structures like aircraft wings, rotor blades, and wind turbine blades. This field investigates the deformation and vibration of these structures resulting from aerodynamic loads experienced during flight or operation. Aeroelastic phenomena comprise various behaviours such as flutter, divergence, control reversal, and gust response. It is paramount to comprehend and mitigate aeroelastic effects to uphold the structural integrity, stability, and performance of aerospace vehicles and systems.

1.4 Multi-fidelity surrogate model through transfer learning

1.4.1 Introduction

Transfer learning is a sophisticated technique increasingly employed to develop multi-fidelity surrogate models, which are essential for efficient and accurate predictions in complex systems. This approach strategically

leverages the complementary strengths of lower-fidelity and higher-fidelity datasets. Initially, a neural network is pre-trained on an extensive set of lower-fidelity data, which, while less precise, provides a broad understanding of the underlying physical phenomena at a significantly reduced computational cost. This phase allows the model to learn fundamental patterns and general features that are relevant across different fidelity levels. During pre-training, the model's architecture captures these broad trends effectively, setting a robust foundational layer of understanding.

Once the pre-training phase is complete, the model is fine-tuned using a smaller, but more accurate, dataset from higher-fidelity simulations. Fine-tuning involves selectively updating the model's weights to align more closely with the detailed and precise characteristics found in the high-fidelity (HF) data. This is typically done by freezing the initial layers, which contain the general features learned from the lower-fidelity data, and only allowing the later layers to be adjusted during fine-tuning. This hierarchical adjustment ensures that the model retains the valuable general knowledge from the lower-fidelity data while incorporating the nuanced details from the higher-fidelity data.

The process of combining these fidelity levels through transfer learning significantly enhances the surrogate model's predictive performance. The pre-trained lower-fidelity model captures broad trends and provides a good approximation, which is then refined and sharpened using the HF data. This two-step training strategy not only improves the model's accuracy but also makes the training process more efficient, as the model does not need to learn from scratch when exposed to HF data.

In practical applications, this approach is particularly valuable in fields such as aerospace engineering, climate modelling, and material science, where HF simulations are computationally expensive and time-consuming. By utilizing transfer learning, modelling experts can develop surrogate models that offer a balanced compromise between computational efficiency and predictive accuracy. The resulting multi-fidelity surrogate models are capable of providing rapid and reliable predictions, facilitating more effective decision-making and optimization in complex systems.

Furthermore, this method enables better utilization of available data, maximizes the insights drawn from HF simulations, and ensures that surrogate models remain robust and generalizable. The combination of transfer learning with multi-fidelity modelling represents a significant advancement in the field, offering a practical solution to the challenges posed by limited HF data and the need for high-precision predictions.

1.4.2 Fidelity levels - which type of analysis is carried out at which fidelity level

Low-Fidelity, physics-based, analytical models

Low-fidelity (LF) models are exploited for their speed and their versatility. Disciplines like Flight Mechanics relies largely on the rigid body equations of motion, which are very simple to implement including the addition of quaternions to avoid the Euler angles singularities. It is therefore an intuitive choice to proceed from a conventional rigid body dynamics approach, enhancing it with more accurate formulations of the aerodynamic forces.

A similar argument can be made for structural dynamics, which builds the base for aeroelasticity. Note that rotor dynamics is a further complication in this case as it carries along gyroscopic and centrifugal terms, additional elastic degrees of freedom and fixed-rotating frame interactions (whirl flutter). All this is more easily managed with an analytical model which takes these phenomena into account exactly, rather than relying on a more complex FEM where dynamic and rotational effects are considered at much higher costs.

Mid-fidelity, physics-based, vorticity solvers

Mid-fidelity (MF) level refers to the so-called vorticity-based solvers, so-called Vortex Particle Method (VPM). These solve the evolution equations for the three vorticity components instead of the Navier-Stokes equations. In most cases, this is done via particle methods thus without a computational mesh. Vorticity particles are introduced into the computational domain as they are needed. The aerodynamic forces on surfaces are

estimated via LF solvers such as panel methods or Vortex Lattice Method (VLM). Such solvers are of course unable to model viscous forces and their effects such as boundary layer separations. Consequently, they are perfectly suited to model vortical flow fields, possibly more than "proper" Navier-Stokes based methods, as long as the flow is attached on all surfaces also because meshless methods can handle rotating systems much better than methods using meshes.

High-fidelity solvers - physics-based, compressibility, viscous stresses etc but no better vorticity resolution
HF solutions are typically those involving the numerical solution of the Navier-Stokes equations either following the Reynolds-averaged Navier–Stokes (RANS), Large Eddy Simulation (LES), Detached Delayed Eddy Simulation (DDES) or other approaches. As is well known, even the finest grid does not allow the conservation of vorticity, whereas mass, momentum and energy are conserved by design. This is particularly evident in vortical flow, as vorticity is inevitably dissipated. Furthermore, the management of rotating geometries (such as it is necessary to model rotors and propellers) requires complex grid manipulations. Whereas RANS or DDES might be perfectly suited to characterize the steady or unsteady aerodynamics of VTOL's wings and fuselages, their application to the solution of the flow around the whole VTOL is very challenging.

1.4.3 Multi-fidelity realization

The idea we followed is quite simple: we enhance the accuracy of LF methods with the aerodynamic forces calculated by MF or HF methods. MF data may even be obtained in real-time, as they are computationally very efficient. However, it is more practical if these values are pre-computed on a given parameter space and interpolated for the parameter combination needed by the LF model. Typically, we can extract rotor forces, wings forces or pressure distribution or vorticity distributions from MF solutions. The dependence of these quantities on the parameters (for instance, these parameters could be forward speed, angle of attack, angle of sideslip, rotors rotational speed can be strongly nonlinear; a simple interpolation technique may not provide sufficient accuracy. For this reason, we relied on Co-Kriging and Neural Networks from the outset.

1.4.4 Steady and unsteady physics

An interesting note concerns the differences encountered in different regimes: whereas the implementation of multi-fidelity methods in steady problems may seem straightforward, its application to unsteady problems does not. Furthermore, implementing the aerodynamic lag of wings may be easy or at least feasible also by non-experts, for instance via the well-known Theodorsen function or a Reduced Order Model (ROM) identified from CFD data - whereas the lag of rotors responses poses more challenges as it is not tabulated anywhere in the literature. The authors intend to create some tables to help deal with this problem and present the results in a publishable format.
In practice: the knowledge of the rotors thrust alone may not be sufficient if RPM or the rotor speed are not constant in time. A few experiments we carried out with MF methods, provide the evidence that the transient effects are substantial. Rotor tend to respond to an RPM increase or to an input signal designed to increase thrust in two phases: a strong thrust increase is initially observed; subsequently, it progressively reduces and reaches a constant value. As far as we can tell, this is not entirely reflected in the literature, as the most studied types of rotors (i.e. helicopters and wind turbines) tend to spin at constant angular velocity (helicopters) or let it change very slowly (wind turbines). This is indeed a new challenge to the designer and is not one that can be overcome with new technology. So far, we could not find any better solution than identifying a ROM for the aerodynamic lag states of each rotor.

1.5 Uncertainties Quantification

1.5.1 Bayesian Neural Networks

Bayesian Neural Networks (BNNs) are a type of neural network that incorporates Bayesian inference principles to model uncertainty in the weights and predictions. Unlike traditional neural networks that produce point estimates of weights, BNNs treat the weights as probability distributions, allowing for the quantification of uncertainty in the model's predictions. This approach provides a probabilistic interpretation of the model parameters, enabling more robust and interpretable predictions, especially in cases where data is sparse or noisy.

BNNs provide a systematic and theoretically grounded method to quantify uncertainty in predictions, which is vital for applications where the reliability of predictions is as crucial as the predictions themselves.

1.5.2 Aleatoric Uncertainties

This type of uncertainty arises from the inherent noise in the data. For example, sensor measurements in flight testing might have noise due to environmental factors. BNNs can model this by incorporating noise directly into the output predictions.

1.5.3 Epistemic Uncertainties

This type of uncertainty is due to limited data and the model's lack of knowledge. It decreases as more data is collected. BNNs capture this by representing the model weights as distributions and updating these distributions as more data is observed. Most importantly, BNNs provide an assessment of the quality of the data and determine whether the quantity of data is sufficient to ensure effective model training.

1.6 Modelling Details and relevance to Special Condition VTOL

1.6.1 Rotor thrust unsteadiness

As mentioned in section 1.4.4, rotor thrust and torque do not react to parameters variations with negligible delay. Indeed this delay may be relevant to characterise the overall dynamic response of the drone. A typical response to a sudden increase of angular velocity may look like the one in Figure 2.

It can be argued that a step variation of angular velocity is not realistic; however, as these rotors tend to be much smaller than conventional helicopter rotors, the reference time of the mechanical response may be comparable to that of the aerodynamic wake. In other words, VTOL propellers may have a dynamic of their own, which can be characterised by time accurate MF simulations. Easy-to-handle state-space systems (for instance) can be identified and implemented into the LF simulations.

1.6.2 Role played by control systems

The interaction between structural dynamics and control system are potentially relevant and must be considered. That said, we noticed a clear separation in the frequency domain between the poles of the control system and those of the aeroelastic part of the system.

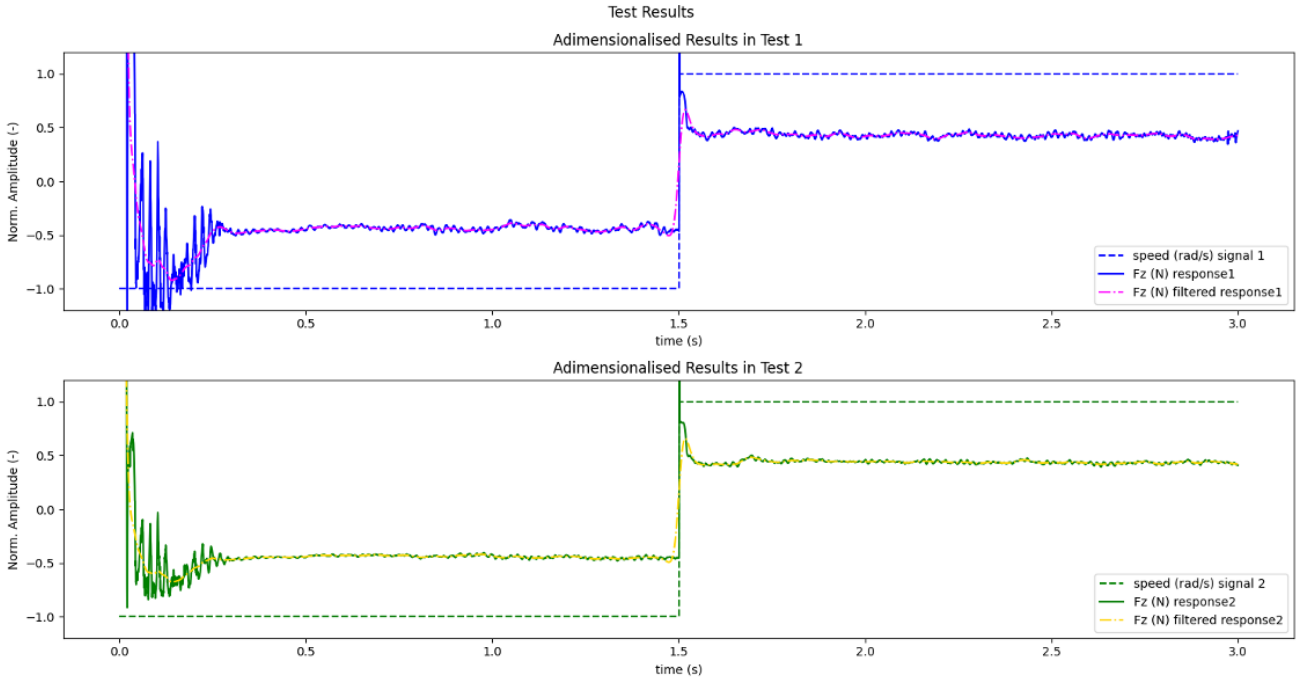

Figure 2: Rotor thrust response to a step variation of angular velocity.

1.6.3 Blades elastic degrees of freedom

VTOL propellers/rotors are tendentially small; the blades are rigidly connected to the rotor head (with no flapping hinges). This implies that a high vibratory level is expected both in the blades and in the rotor head. In our opinion, the interaction between rotating and non-rotating degrees of freedom must be considered. A conventional approach consists in using the so-called multi-blade coordinates (refer for instance to [4]).

1.6.4 Influence of rotors and blade elasticity on wing's aeroelastic response

Whirl flutter

The best known detrimental effect of the rotating - nonrotating interaction is represented by whirl flutter, which happens when some of the rotating modes couple with the modes of the structure holding the rotors. As far as we can assess, this threat is unlikely to happen on properly designed systems. However, it may become an issue on a damaged system. This confirms the necessity to incorporate the rotating degrees of freedom.

Dynamic loading on surrounding structure

The rotors rotation generates dynamic loading on wings and supporting structures. This is potentially relevant to the vibrational level and the damage the material may suffer. These effects are potentially much greater on damaged configurations.

Dynamic loading on rotor blades

Dynamic blade loading is also relevant to assess the potential damage in blades material. These effects are potentially much greater on damaged configurations.

1.6.5 Role played by Artificial Intelligence

With reference to EASA AI concept paper, our approach only exploits AI to level 1, i.e. as cognitive assistance, as a support and help to the drone developers to produce data with higher quality and more easily.

When AI serves as cognitive assistance, it offers valuable insights and recommendations to augment human decision-making capabilities. These systems provide relevant information, suggest options, and automate routine decisions, thereby enhancing the efficiency and effectiveness of decision-making processes. While AI can actively participate in decision making, the extent of its involvement varies. However, it's important to note that these systems do not make decisions independently; they operate within predefined parameters and guidelines.

2. Methodologies

This section is about the methodologies applied to build our comprehensive Flight Simulation Model (FSM). This project investigates a combination of methodologies to generate reliable and practical flight load envelopes for our multi-rotor eVTOL aircraft. The study aims to model a vast range of potential configurations, control strategies, flight conditions, and individual rotor variations in speed and acceleration, encompassing both normal and failure scenarios.
Our proposed approach starts from LF physics-based models and a few HF data points to build and continuously improve data-driven models throughout the development, certification, and operational lifespan of the eVTOL. This iterative process leverages both numerical simulations and experimental data as it becomes available. Notably, there is no final data-driven model, i.e. the DT will be designed to adapt to customizations and re-configurations of the aircraft, ensuring its continued relevance throughout the vehicle's lifecycle.

2.1 Flight Simulation Model architecture

A modular approach is a design strategy that splits a system into independent, self-contained modules, each with specific functions and interfaces. This modularity enhances flexibility, scalability, and reusability, simplifying the management and adaptation of complex systems. Modular approaches are particularly valuable when multiple disciplines are involved. Additionally, and particularly relevant to this project, is the potential to substitute one or more modules with a data-driven model. Figure 3 display the comprehensive modelling strategy. The Flight Mechanics module is found on the left side, while the Aeroelastic module (dynamic stability) is on the right. The former module is built to analyse comprehensively the rigid-body flight mechanics and dynamics of the eVTOL. During the preliminary analysis of flight tests, it was found out that the rigid body and elastic modes are sufficiently separated in frequency, allowing the Flight Mechanics and Aeroelastic modules to be treated independently.

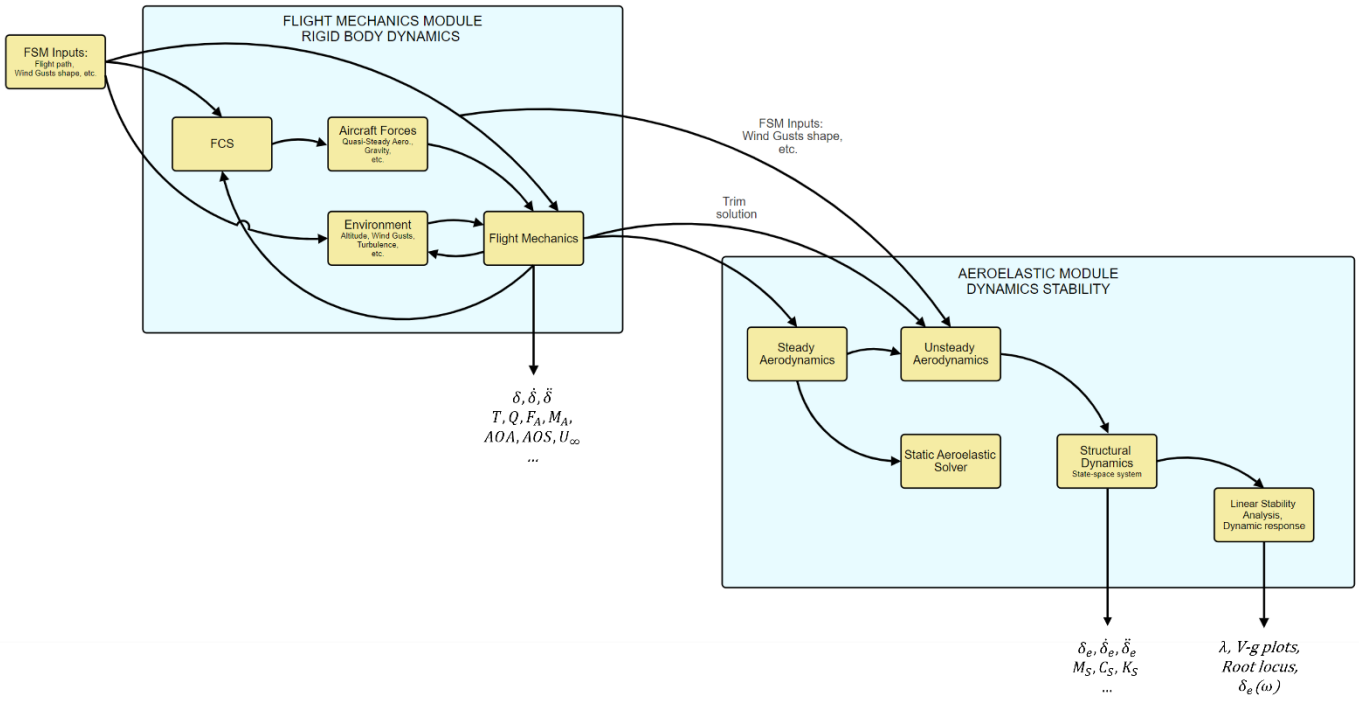

Figure 3: Comprehensive modelling strategy.

On the other hand, the aeroelastic analysis is therefore designed to deliver static deflections, linear stability and linear stability margins, and dynamic response. The latter can be based on the linearized system (in time or frequency domain) or on the time integration of the fully nonlinear one.

2.1.1 Flight Dynamics module

A LF flight simulation model of the entire vehicle has been implemented in MATLAB® Simulink®. The model consists of modules that simulate the various systems as well as the physics acting on the vehicle. The modular approach allows replacing individual components of the model, for example with higher fidelity versions or even with surrogate models of said component. An overview of the model structure is shown in Figure 4. The LF implementation of the modules will be described in the following section. Interfaces were created, that allow to use the simulation model for various purposes, such as determining trim conditions, linearizing the system, or performing full flight simulation.

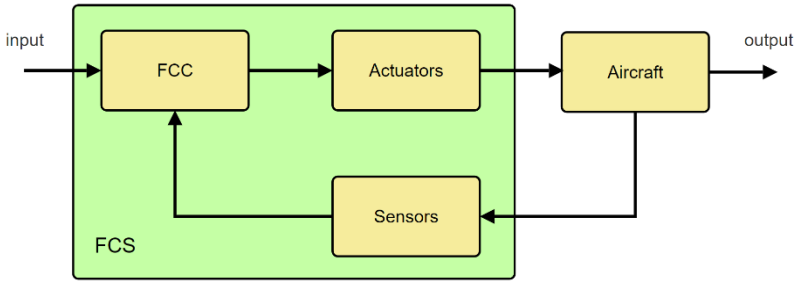

Figure 4: Model structure of the MATLAB® Simulink® model.

2.1.1.1 Components

2.1.1.1.1 Aircraft

The “Aircraft” module contains the main flight mechanics of the vehicle. It includes simulation of the equations of motion, the aerodynamics, the propulsive system, the structure as well as an atmospheric turbulence model. For the LF implementation, the aerodynamics of the wing and tail, including the control surfaces, were modelled using a VLM. One of the main limitations of this method is that it is only applicable for small angles of attack and angles of sideslip. The aerodynamic coefficients at high angles of attack were therefore extrapolated, similar to the method suggested by [5,6].

The thrust and torque of the propellers were modelled using test data measured from the real propellers. While this model allows accurate simulation of an individual propeller’s performance, it does not account for the effects of the complex airflow interactions between the various components.

The LF structural model only simulates the wing bending as a rotation of the wings about the wing root, by modelling a damped sprung mass for each wing.

The atmospheric model allows changing the environmental conditions, such as air temperature, density and pressure. Air turbulence can be simulated as well, using the Dryden form of the spectra for the turbulence as described in [7].

2.1.1.1.2 Actuators

The actuators for the ailerons and ruddervators are modelled as simple low-pass filters. Their bandwidth and rate limits have been chosen to represent the typical characteristics of a scale model actuator, such as the ones used in Skiron-X.

2.1.1.1.3 Flight Control Computer

To model the flight control computer, two sets of cascaded PID control loops have been implemented. One set is used when the vehicle is in helicopter mode. It controls the vehicle's attitude, primarily using the throttle of the four hover propellers. The other set controls the vehicle in airplane mode, using the pusher propeller and the aerodynamic control surfaces.

2.1.1.1.4 Sensors

The sensors of the vehicle have been modelled as low-pass filters with transport delays. Again, the characteristics of the filters have been chosen such as to represent the qualities of sensors typically used in this application.

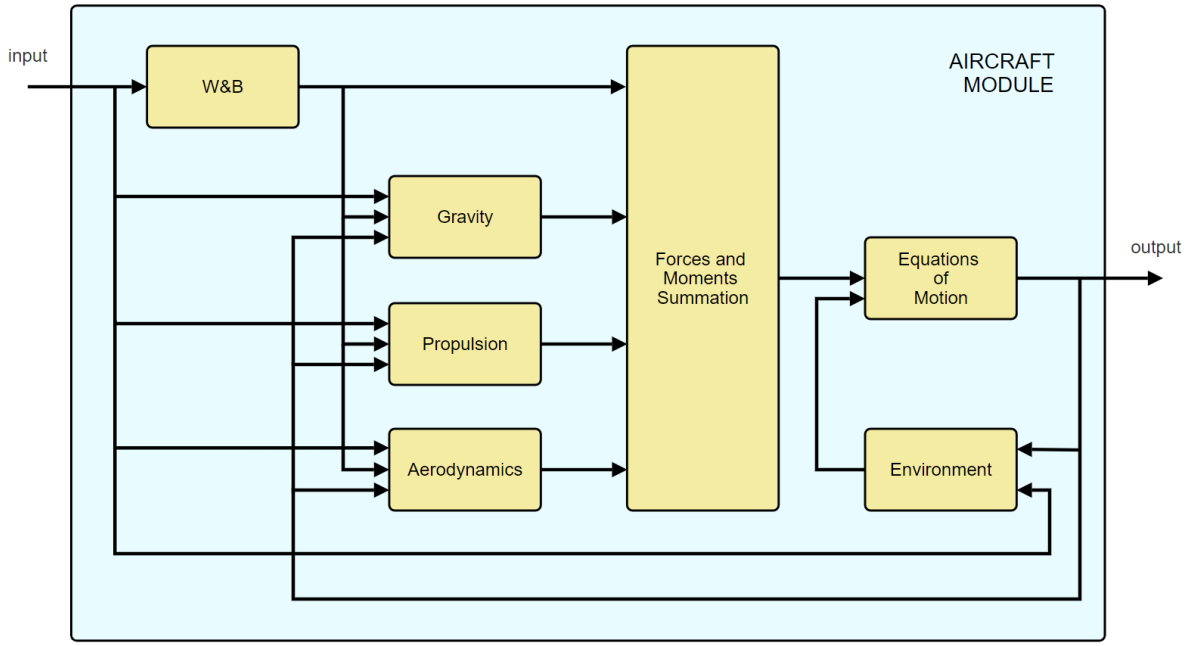

Figure 5: Aircraft model architecture.

2.1.1.2 Functionalities

The model can also be used to perform full flight simulations. Furthermore, a series of tools has been developed to interface with the Simulink® model. A trim algorithm can be used to determine the states and control inputs to achieve a desired trim condition. For example, given a desired bank angle, airspeed and altitude, the algorithm will determine the required pitch attitude, angle of attack, rotational rates, control surface deflections and pusher motor RPM to maintain a coordinated turn under the defined conditions.
A linearization algorithm is then able to linearize the system around a trim condition, allowing it to be expressed in a linear, time-invariant state-space representation. This linearized system can then be used to extract transfer functions and determine stability margins of individual components or of the system as a whole.
Finally, individual components of the model can be replaced with different versions, such as higher fidelity or surrogate versions. The aforementioned tools can still interface with the upgraded model, allowing to perform comparisons between the different fidelity levels.

2.1.2 Aeroelastic module

The flow chart presented here shows the information flow between the different modules used in the simulation. Figure 6 shows the aerodynamic modelling. It is split between steady and unsteady. Whereas the steady aerodynamics modelling relies on the multi-fidelity surrogate model to estimate the rotor thrust values (and, possibly, also wing lift and drag), the unsteady formulation requires a dedicated addition to keep into account the aerodynamic lag. In the flowchart we only show the time domain option, with the state-space formulation, but a formulation in the frequency domain would also be feasible. The state-space formulation can be extracted directly from Theodorsen's theory and corrected or replaced by reduced-order models directly identified from CFD (wings) or MF simulations (rotors).
According to this approach, the steady aerodynamic forces are nonlinear (the MF surrogate model is nonlinear by design) whereas the unsteady formulation is linear. As such, static aeroelastic solutions are nonlinear whereas the stability analysis relies on a linear (linearized) formulation; this is consistent with the conventional approach to aeroelastic analysis mostly used in the fixed wing world. Indeed helicopter engineers may also rely on Floquet analysis.

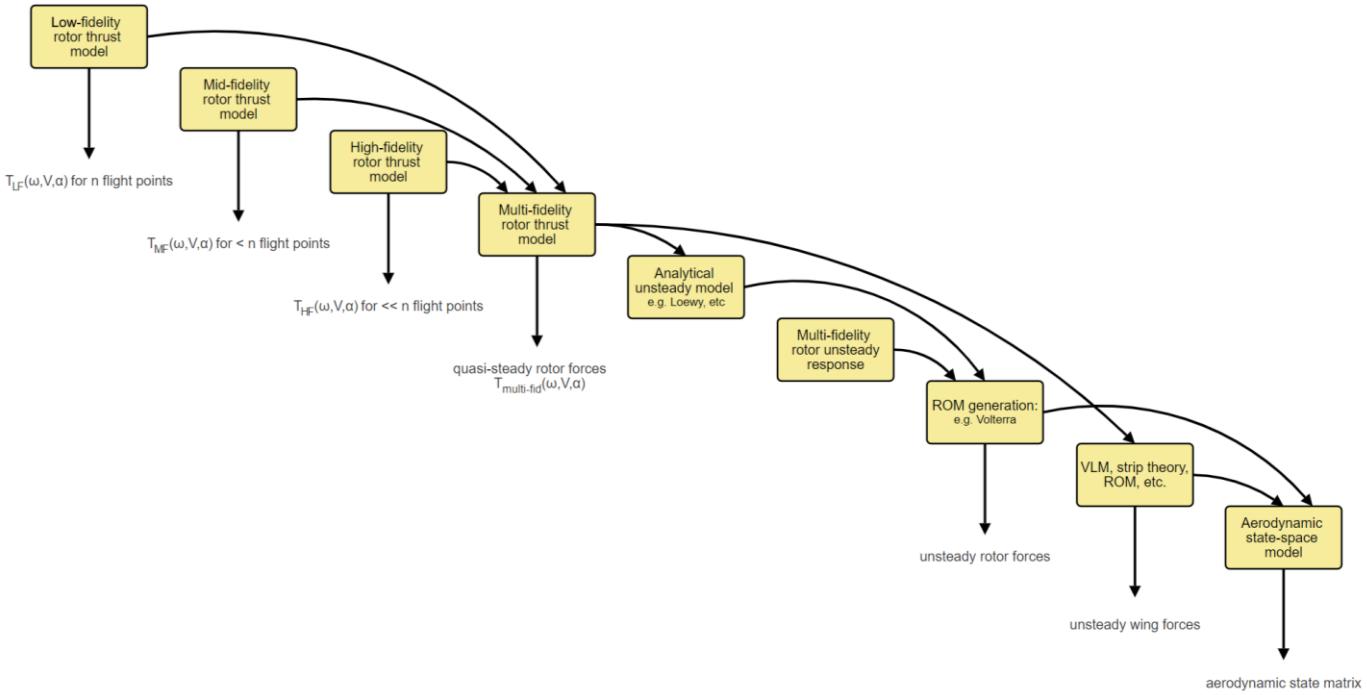

Figure 6: Steady and unsteady aerodynamic modelling flowchart.

Figure 7 describes the structural modelling. Compared to the aerodynamic modelling approach, it is more straightforward, relying on FEM and modal condensation. Geometric nonlinearity can be considered in the static solution.

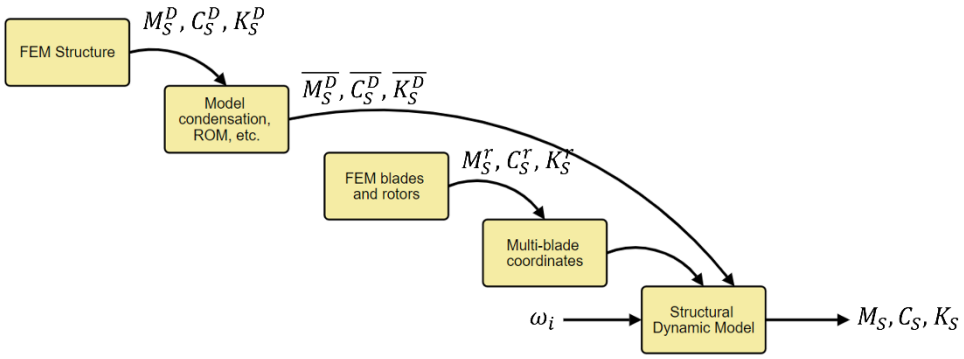

Figure 7: Structural modelling flowchart.

2.2 Low-Fidelity model

2.2.1 Structural model

The structure of Skiron-X is a FEM model constructed using wire modelling techniques, incorporating 32 beam elements resulting in a simple aircraft representation. The structural beam model discretizes the eVTOL into a system of interconnected finite elements, i.e. beams and nodes, where each has assigned specific properties like stiffness and inertia. These proprieties were initially guessed based on our prior experience and later adjusted with flight test data. The governing equations of motion are a classical 2nd order system:

$$\mathrm{M}\ddot{\mathrm{x}} + \mathrm{C}\dot{\mathrm{x}} + \mathrm{K}\mathrm{x} = \mathrm{f}(\mathrm{t}) \tag{2.1}$$

Where M, C and K are the mass, damping and stiffness matrices, respectively, while x and $\mathrm{f}(\mathrm{t})$ describe displacement and external forces.
In addition, our focus was directed towards optimizing computational efficiency. Since an excessive number of degrees of freedom could be detrimental to the simulation performance, a modal condensation technique was implemented. This process involved condensing the structural dynamics into a reduced set of modes while preserving accuracy.

2.2.1.1 Modal Condensation

Using the mode shapes (i.e. eigenvectors) of a structure and putting them all in a matrix as columns builds the modal matrix Φ, which is needed for the transformation into modal coordinates. Firstly, define a coordinate transformation based on the modal matrix and 'modal' (or 'principal') coordinates q, namely

$$x = \Phi q \tag{2.2}$$

Substituting x with Equation 2.2 in the 2nd order equation of motion (Eq. (2.1)) and pre-multiply by the transpose of the modal matrix leads to:

$$\Phi^T \mathrm{M}\Phi + \Phi^T \mathrm{C}\Phi + \Phi^T \mathrm{K}\Phi = \Phi^T \mathrm{f} \tag{2.2}$$
$$M_q\ddot{q} + C_q\dot{q} + K_q q = f_q \tag{2.3}$$

Where

$$M_q = \Phi^T \mathrm{M} \Phi, \;\; C_q = \Phi^T \mathrm{C} \Phi, \;\; K_q = \Phi^T \mathrm{K} \Phi, \;\; f_q = \Phi^T \mathrm{f} \tag{2.4}$$

The matrices M_q , C_q , K_q are known as the modal mass, damping and stiffness matrices, and f_q is the modal force vector. It can be shown that the modal mass and modal stiffness matrices are actually diagonalized (i.e., uncoupled), with the diagonal elements equal to the modal mass m_j and modal stiffness k_j for the jth mode. This diagonalization occurs because the modes are "orthogonal" with respect to the mass and stiffness matrices. This is an extremely useful feature, as will be illustrated later.

The properties of the modal damping matrix present a nuanced picture. If the physical damping matrix C can be expressed as a linear combination of the physical mass and stiffness matrices (M, K), then damping is proportional, resulting in a diagonal modal damping matrix C_q. However, if the damping is not proportional, the modal damping matrix will include cross-coupling terms between modes. During the initial analysis, it is common to assume proportional damping to ensure that the equations of motion expressed in "modal space" in Equation 2.4 are completely uncoupled. The effectiveness of the modal transformation defined by Equation 2.3 becomes apparent when formulating the modal equation of motion for the jth mode in Equation 2.4, assuming proportional damping, so that

$$m_j \ddot{q}_j + c_j \dot{q}_j + k_j q_j = \; f q_j \; for \; j = 1,2, \dots, N \tag{2.5}$$

where m_j , c_j , k_j and $f q_j$ are the modal mass, damping, stiffness and force for the jth mode. Using the SDoF concepts, the damping ratio for each mode is then given by $\zeta_j = c_j/(2 m_j \omega_j)$, where $\omega_j = \sqrt{k_j/m_j}$ is the jth mode natural frequency.

The coupled MDoF equations of motion, originally derived in physical coordinates, are now expressed as a set of uncoupled SDoF equations in modal coordinates. An MDoF system can now be treated as a summation of SDoF systems. All SDoF concepts can then be applied to each modal equation, and Equation 3.2 can be used to combine the modal results back into physical coordinates.

Working with modal coordinates in systems with a significant number of degrees of freedom and, consequently, numerous vibration modes, offers an additional advantage. It allows for a significant reduction in the number of modes considered in a solution. Given the limited frequency range of interest, it is advantageous to reduce the analysis by focusing only on a subset of modes through modal transformation. This eliminates the effects of higher frequency modes. It is common practice to include modes with eigenfrequencies slightly higher than the maximum frequency of interest to account for possible residual effects. Consider limiting the inclusion to n (< N) modes; thus, $\phi_n = [X_1 X_2 \dots X_n]$ would represent the reduced modal matrix, and the transformation to the reduced set of principal coordinates would be

$$x = \phi_n q_n \tag{2.6}$$

As a result, the final set of transformed equations would be simplified to n instead of N Single Degree of Freedom equations.

2.3 Mid-Fidelity

The first modelling improvement is performed by grasping a VPM, a MF solver class. The open-source code DUST [8] has been used to achieve more accurate predictions of the flow through and around the rotors. VPM methods are particularly suitable at capturing vortical flows, a crucial aspect of rotorcraft aerodynamics. By improving the accuracy of rotor wake predictions, we expect to capture rotor-rotor and rotor-wing interactions with greater fidelity. To validate this approach, we conduct a series of unsteady simulations across the entire flight envelope, with a particular focus on "corner cases" where traditional LF methods are known to have

limitations. To strengthen our MF results, the vehicle geometry has been modelled in another VPM-based solver as well, namely FlowUnsteady [9].
Despite delivering both similar results, our aerodynamic database is based on DUST, which offers multiple options for the prediction of the forces over aerodynamic surfaces.

2.4 High-fidelity

Two different approaches were chosen, one based on a cloud virtual wind-tunnel developed by Airshaper [10] and the other employing standard CFD methods (ANSYS Fluent and CFX [11]).

The first approach can potentially reduce the human effort drastically, by automating several pre- and post-processing tasks. The user has only to upload the eVTOL geometry, define the flow conditions and choose the grid refinement level. The software is built to create and clean a watertight geometry even by starting from a geometry with some defects. Depending on the user case, it automatically creates the flow domain size and boundary conditions by choosing if the vehicle is moving on the ground or in the air. In addition, it automatically selects the appropriate turbulence models, here the k-omega SST. The gris is generated automatically through the well-known SnappyHexMesh and is additionally improved thanks to an adaptive mesh refinement scheme. The refinement is adjusting both the volume and surface mesh based on the curl of the velocity field. More information about this can be found in the work of Remmeire and Majksner [12].

On the other hand, the more classical approach is to take advantage of CFD by using standard application software like ANSYS Fluent [11]. The authors grasped CFD on several complexity levels. Since a 3D simulation of a complete aircraft can be computationally expensive, it was decided to simulate first the eVTOL and a propeller separately. It gives us the advantage of familiarizing with meshes and finding the best trade-off. Firstly, the eVTOL was simulated in AP mode without the propellers to obtain a baseline for force and moment coefficients. In addition, the propellers were simulated independently with a multiple-domain approach, therefore resolving the flow over blades.
After this phase, it was decided to simulate the entire aircraft. The challenges associated with this kind of simulations are mostly related to the high computational costs. To obtain the results of a single operating condition, several days on an HPC cluster were needed.

However in all the cases, the following strategy was followed. The commercial Navier-Stokes solvers ANSYS Fluent was used in the preliminary phase. For benchmarking purpose, simulations were conducted and CFX were used as main CFD solvers. The following two turbulence models were used in this study:

- Spalart-Allmaras (SA) Model as default
- Transition SST k-omega model for turbulence model study

2.5 Flight Test

The eVTOL selected is a simple configuration equipped with static lift and cruise rotors. It is an Unmanned Aerial Vehicle (UAV) called Skiron-X and operated by Aurora Flight Sciences. It has been developed to easily takeoff and land vertically and to perform sustained endurance fixed-wing flights. It has been developed to easily takeoff and land vertically and to perform sustained endurance fixed-wing flights. The vehicle length and wingspan are about 2.2 and 5 m, respectively, and weighs 22 kg. It can fly at maximum forward speed of 26 m/s and about 3 hours in fixed-wing flight. It has four longitudinal-symmetrical placed rotors, in front and behind the wing, which serve as lift devices for Helicopter (HC) mode related activities, such as takeoff/landing, hovering and ascent/descent. On the other hand, behind the eVTOL tail, it is present one single pusher propeller, which is used in Airplane (AP) mode as a forward thrust device.

To validate our FSM, flight tests were carefully planned and performed. The eVTOL was equipped with several sensors, including accelerometers and strain gauges to characterize the structural response of the eVTOL. Maneuvers in both HC and AP modes were conducted trying to cover the whole flight envelope.

2.6 Multi-fidelity surrogate model

The use of AI/ML techniques is associated to the high computational costs needed with running numerous, HF simulations for many flight conditions. These HF simulations are capable of generating accurate results but are also computationally expensive. Specifically, predicting aerodynamic loads through numerous CFD simulations for a vast range of flow conditions becomes impractical. To address this challenge, data-driven models have been built in mainly three different ways. As highlighted in the deliverable D-1.1 [1], Gaussian Process (GP), ROM and Neural Networks (NN) were recognized as the most useful techniques.

The first technique employed to reduce computational costs is the use of ROMs. They offer a way to significantly reduce the complexity of HF models by decreasing their degrees of freedom, essentially the number of variables needed to describe the system behaviour. This simplification process leads to a more computationally efficient model, while still maintaining an acceptable level of accuracy compared to the original complex system. Various algorithms can be exploited to generate ROMs, such as Proper Orthogonal Decomposition (POD) and Dynamic Mode Decomposition (DMD). These algorithms identify the dominant features or modes that capture the most important dynamics of the original system, allowing a more efficient prediction.
GP are a type of stochastic model that utilizes functions to represent a dataset. The two key components are the mean function and the covariance function. The former captures the average behaviour of the data distribution, while the latter, as known as kernel function, defines how the functions vary across different data points, essentially describing the relationships between them. The inherent strength of GP lies in their ability to predict not only the evolution of observed data but also its associated confidence level. This makes them particularly suitable for tasks like regression, interpolation, and uncertainty. Within the framework of our research, GP regression emerges as a valuable tool to address computational cost limitations. GP regression involves fitting a function (often referred to as Kriging) to the observed data. This method leverages the spatial relationships between data points, whether in terms of distance or direction, to explain observed changes or differences within the data space.
Another approach for generating predictions based on datasets involves NN. There are many different data processing techniques and they have become well-established tools within industry for various applications. NNs are composed of interconnected layers, each containing artificial neurons. The input layer typically receives raw data points relevant to the problem, such as speed, density, and temperature. As data progresses through the network, hidden layers act as intermediate processing stages, performing calculations on the weighted sum of inputs from the previous layer. These calculations are then passed through an activation function, introducing non-linearity and allowing the network to learn complex relationships between input and output data. Finally, the output layer delivers the desired results, such as aerodynamic coefficients. A crucial aspect of NNs lies in the training process. During training, the network iteratively adjusts the weights associated with connections between neurons. This optimization aims to minimize the difference between the network's predictions and the actual data (training dataset), ultimately enabling the NN to learn the underlying trends within the data.
However, relying solely on surrogate models can be insufficient in complex scenarios where the input-output relationships are highly non-linear, leading to unreliable results. This is where Data Fusion (DF), a branch of ML/AI, comes into play. By combining the strengths of both HF and LF models, DF techniques aim to generate accurate and reliable results compared to using either approach individually. Depending on the leveraged ML technique, many different approaches are known. For GPs, co-Kriging is chosen for the sake of its simplicity and applicability. This technique allows us to fuse the data of different fidelities together and assess the uncertainty.

When employing NNs to fuse the data together, a technique called Transfer Learning (TL) is needed. This approach utilizes a Deep Neural Network (DNN) trained in stages to leverage both LF and HF data effectively. In the first stage, a large, unconstrained network is trained on the LF data. This initial training guides the model towards a promising region of the solution space and we actively monitor to avoid overfitting. A second stage employs TL to improve the take advantage of MF and HF data. Here, we transfer the knowledge gained from the LF data (weights of the neurons) to a new network and fine-tune it with a subset of the more expensive MF and HF data. Finally, in the last stage, specific parts of the network are frozen, while the remaining layers are further trained with adjusted hyperparameters. This final stage allows the model to refine its predictions and achieve a more accurate fit to the complex HF data points. Overall, this multi-stage training strategy aims to accelerate the model's convergence towards a better solution by leveraging the strengths of both LF and MF data. The process is shown in Figure 8.

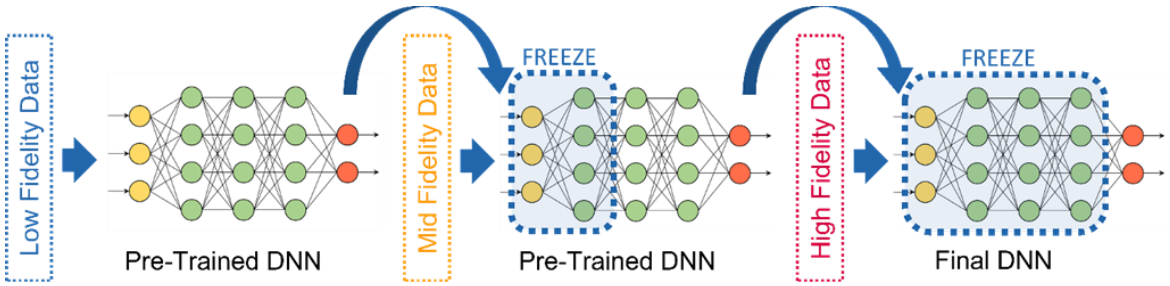

Figure 8: DNN data fusion framework [13].

On the other hand, to assess the uncertainty, a statistical method called Bayesian Neural Network (BNN) is integrated within the ML framework. Instead of assigning a single, fixed value to each model parameter (e.g., neuron weights), these parameters are characterized by probability distributions. This probabilistic framework allows for the quantification of epistemic uncertainties, which arise from our limited knowledge of the underlying physical phenomena. A figure of the NN is depicted in Figure 9.

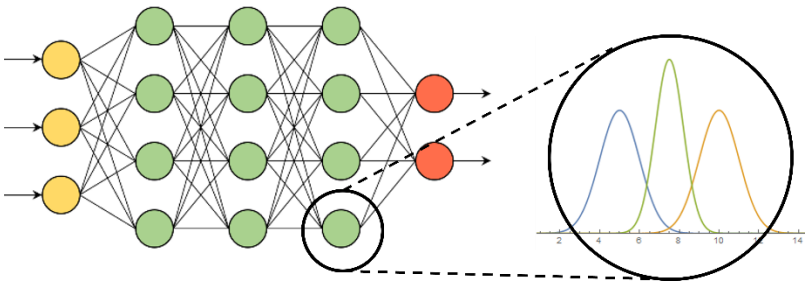

Figure 9: Bayesian Neural Network based on probability distribution [13].

Finally, the two methods are joined together to obtain a robust approach to deal with data fusion and uncertainty quantification, here named BNN-TL (see Figure 10). More information are available in the work of Vaiuso et al. [13].

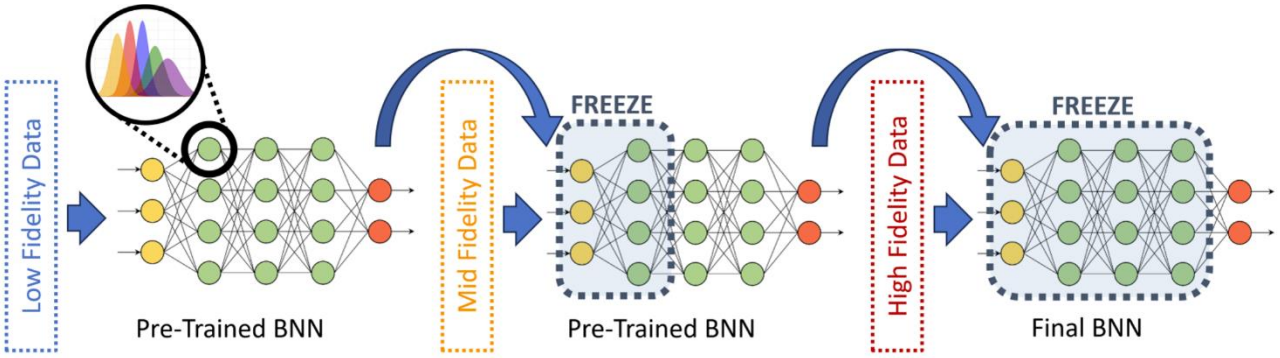

Figure 10: Bayesian Neural Network with Transfer Learning framework [13].

2.7 Uncertainties quantification

A critical aspect of this research lies in ensuring the trustworthiness of our DT predictions. Uncertainty Quantification (UQ) plays a vital role in achieving this goal. UQ allows us to identify regions within the input space where the DT predictions might be less reliable. These areas of potential unreliability could arise from limited data availability and high variance in the data. Our work focused mainly on aleatory and epistemic uncertainties.

Our research acknowledges the inherent variability and randomness (aleatory uncertainties) present in both the eVTOL aircraft itself and its operating environment. Assuming perfect knowledge of these factors would be an unsafe presumption. Unforeseen events or unknown factors can always lead to unpredictable behavior in the system. For the eVTOL, aleatory uncertainties can arise from various sources, as slight variations in the manufacturing process can lead to differences in material properties, weight distribution, and other factors that can influence flight dynamics. Even within a specified material type, there can be inherent variations in properties like strength and elasticity. These variations can impact the eVTOL structural integrity and response to external loads. Environmental factors also contribute to aleatory uncertainties, like inaccuracies in pressure and temperature measurements can lead to deviations from predicted flight performance.

To address these uncertainties, particularly when limited data is available, we plan to employ forward propagation techniques. Several methods are viable for forward propagation, including Monte Carlo simulations and Polynomial Chaos Theory [14]. The former involves running numerous simulations with random variations in the input parameters to assess the range of possible outcomes. The latter offers a more efficient approach compared to Monte Carlo simulations using a mathematical expansion to represent the effects of uncertainties on the outputs. Previous research by NASA [15] and our own group [16] has demonstrated the successful application of non-intrusive polynomial chaos expansions for uncertainty propagation in aeroelastic problems.

The second category of uncertainties we consider are epistemic uncertainties. These arise from limitations in the method itself, and can be reduced by employing more complex models that better capture the system behaviour or by acquiring more data for specific conditions. In the context of aerodynamics, epistemic uncertainties arise from turbulence modelling and flow unsteadiness. To quantify these uncertainties, GPs and BNNs are particularly well-suited. Both methods provide predictions with a mean value and a corresponding variance, allowing for a straightforward assessment of the model confidence.

Both aleatory and epistemic uncertainties contribute to the construction of a "confidence interval" around the predicted mean value. This interval is typically defined by a certain variance range, often including 95% of the possible predictions. Knowing the size of this range, which reflects the spread of potential outcomes, provides valuable information for decision-making. By analysing the confidence of the applied methods and procedures,

this research aims to determine their effectiveness for broader applications, potentially including certification purposes. By incorporating both uncertainties into our analysis, we aim to develop a more robust and reliable understanding of the eVTOL behavior under various conditions.

3. Results and Discussion

3.1 Models development

This section summarizes the various model developments, from structural to aerodynamic.

3.1.1 Structural model

The structural model of Skiron-X was reduced thanks to the model condensation technique. Thanks to a finite element analysis, our system passed from 2697 physical degrees of freedom to be effectively evaluated with only 20 (n) modal equations, demonstrating substantial computational efficiency gains without sacrificing model fidelity.

To validate the model we took advantage of flight test data. In particular, the strain gauge data collected during flight was leveraged. By subjecting this data to Fourier Transform analysis the eigenfrequencies of crucial structural modes specifically, the first two bending modes and the first torsion mode were extracted. These eigenfrequencies served as crucial benchmarks for the model. To ensure that the simulated eVTOL exhibited responses akin to its physical counterpart, wing profiles were meticulously tailored to match these eigenfrequencies. This approach facilitated the replication of critical dynamic characteristics observed during flight operations.

The measured data from accelerometers and strain gauges were used to analyse the structural dynamics of the wing. Specifically, four strain gauges were strategically positioned on the wing, with two dedicated to measuring bending moments and the remaining two for torsional forces. Grasping the data collected from strain gauges, Fast Fourier Transform (FFT) analysis was employed to extract valuable frequency domain information. The primary objective was to identify the eigenfrequencies characterizing the structural modes of the wing.

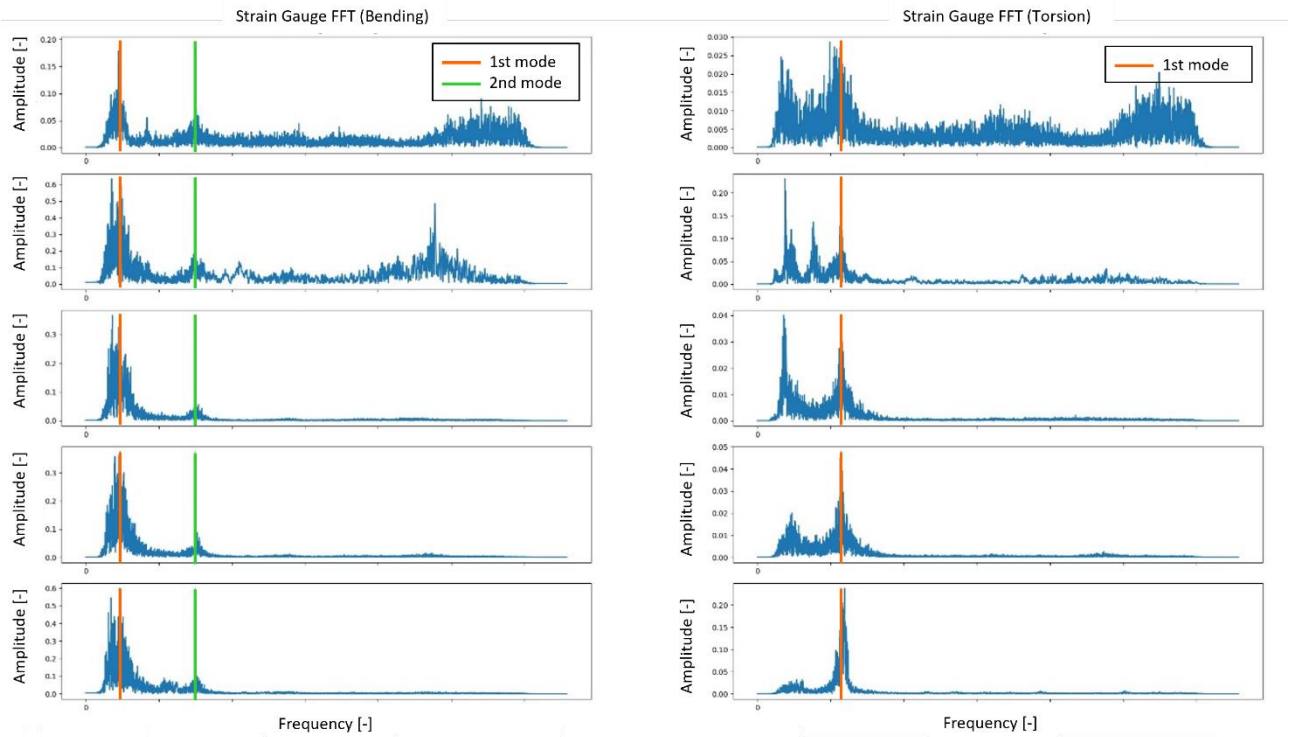

Figure 11: Strain gauges FFT analysis for bending moment and torsion dynamics (left and right).

Analysis of the FFT results revealed prominent eigenfrequencies corresponding to critical structural modes (see Figure 11). Notably, two distinct bending mode shapes were observed (red and green lines), while a torsion mode shape was identified (red line). Additionally, several minor peaks were detected in the frequency spectrum, albeit with challenges in precise definition. Overall, the FFT analysis of the strain gauge data provided valuable insights into the dynamic behaviour of the wing during flight, highlighting key eigenfrequencies associated with bending and torsional modes, essential for structural assessment and model validation.

3.1.2 Mid-fidelity

As explained in the section 2.3, the popular VPM-based open source code DUST [8] was chosen as mid-fidelity solver. It offers multiple methods to calculate forces and moments produced over an aerodynamic surface, from the fast Lifting-Line (LL), to standard VLM and non-linear (NL) VLM and a surface panel (SP) method. In addition is it also possible to introduce bluff bodies, for example, to account for the fuselage.

Propeller modelling

Based on some preliminary simple benchmark cases, the best approach to model the propellers was with the NL-VLM. The LL method suffered from numerical instabilities, while both standard VLM and SP were not able to capture viscous effects. The decision was taken due to the broad flight envelope of the eVTOL, where during both HC mode and transition the local angle of attack (AOA) on the propeller blades could be very high or low. The non-linearities are accounted for by providing aerodynamic correction tables. They were built with LF methods, namely XFoil [17], and extrapolated at high angles of attack with the Viterna method [6]. The software Qblade [18], a muti-physics simulation package, was used to create the look-up tables for different Mach and Reynolds values. Two examples are displayed in Figure 12. They show the lift coefficient (CL) of one blade section of one lift propeller and pusher propeller at one Re and several Ma numbers (left and right, respectively).

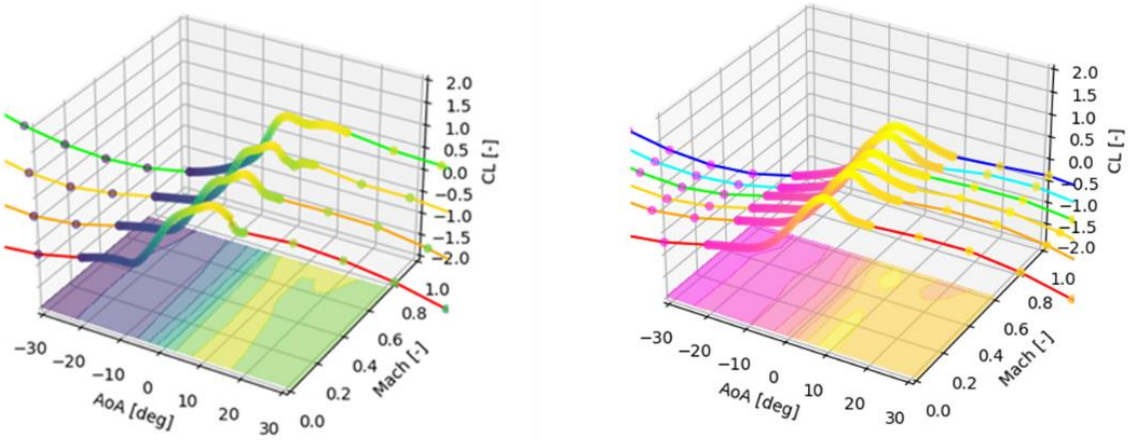

Figure 12: Aerodynamic-table data example for a lift-propeller section (left) and for a push-propeller section (right)

To validate the prediction of the propellers and of the NL-VLM, a comparison with the manufactured data was performed and shown in Figure 13. On the left and right, respectively, one can find the results for the lift and pusher propeller. Similarly, the use of the NL-VLM slightly improves the prediction in comparison to the validation data (experimental and manufacturer data). However, this data is only available without any relative wind speed condition and but only by varying the rotational speeds. In our case, since the operating conditions of the eVTOL vary largely resulting in very low and high AOA, AOS, freestream velocities and rotational speeds, we expect to obtain more reliable results even outside this narrow validation dataset.

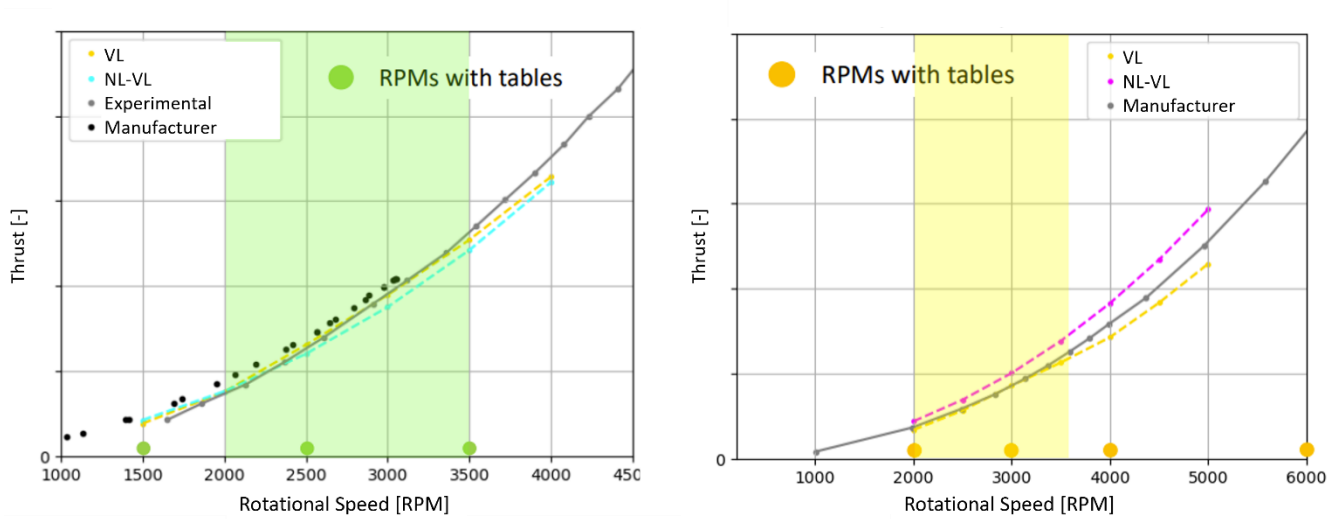

Figure 13: Validation of NL-VLM of lift and pusher propeller (left and right).

Aircraft modelling

The complete model implementation started with a comparison between the available methods. Our first attempt was to model the eVTOL at the highest fidelity possible, i.e. all the aerodynamic surfaces (wings and ruddervators) and the fuselage were modelled with the SP method (see Figure 14).

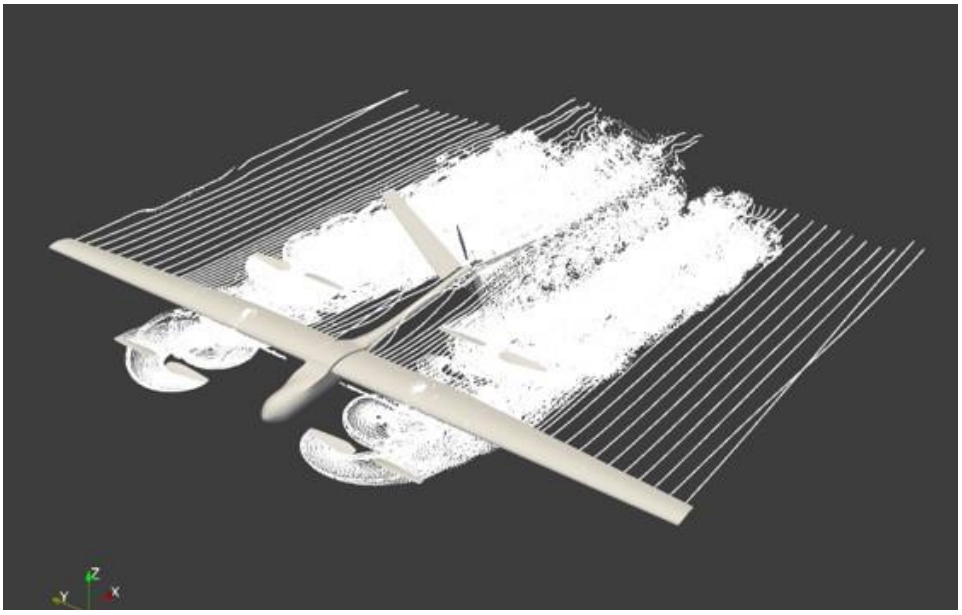

Figure 14: Initial DUST model, with fuselage.

Due to the high computational cost of this approach, it was decided to simplify the model by neglecting the fuselage and using the NL-VLM for the wing as well (see Figure 15). The exclusion of the fuselage was motivated by the high element density of this component which has a secondary role in the eVTOL aerodynamics.
The simplification of the model reduced the simulation times from dozens of hours, even days; to a few hours. Considering that the goal of this model is to explore an important amount of operating conditions, only a few hours of computational time were considered reasonable. It allowed us to calculate several important points of the flight envelope.

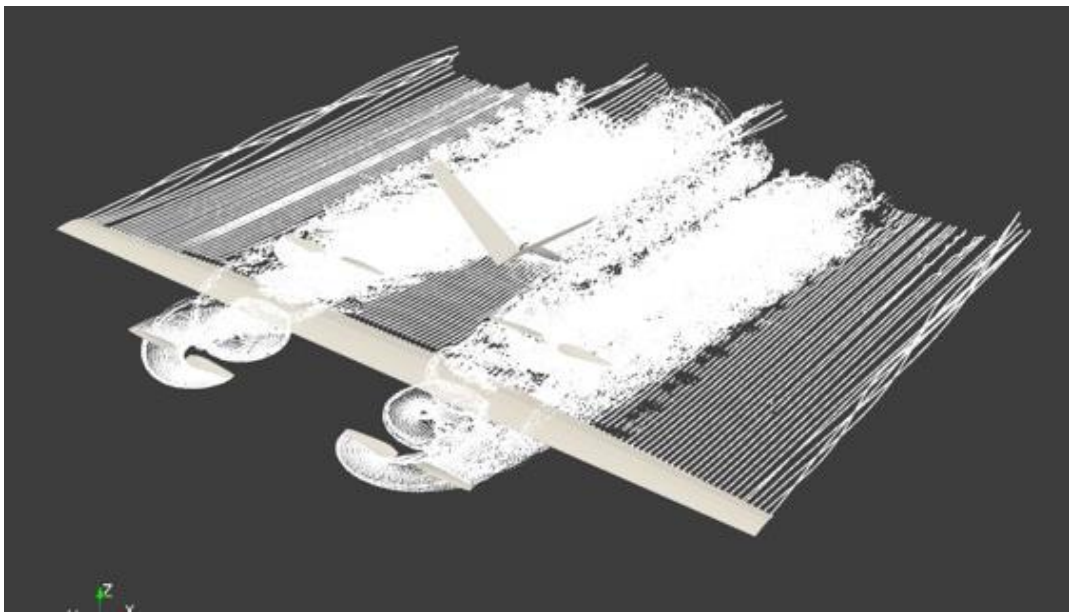

Figure 15: Final model used for building the database.

In any case, a systematic comparison between the available modelling methods and approaches was performed. The first comparison is about the influence of the fuselage on the forces and moments produced by the propellers and the wing. The following results are the outcome of DUST simulations in a "transition-like" phase:

- the UAV is flying at a speed near the stall
- the lift propeller at around 50% of max rotational speed
- pusher propeller near max rotational speed

Figure 16 shows the load distribution over the wing with and without the presence of the fuselage (respectively in cyan and red). The complete model with the fuselage yields a force drop over the wing center, which is physically reasonable since the fuselage itself is not contributing so effectively as a wing. However, the distribution in the portion just behind the propeller is similarly affected by both approaches.

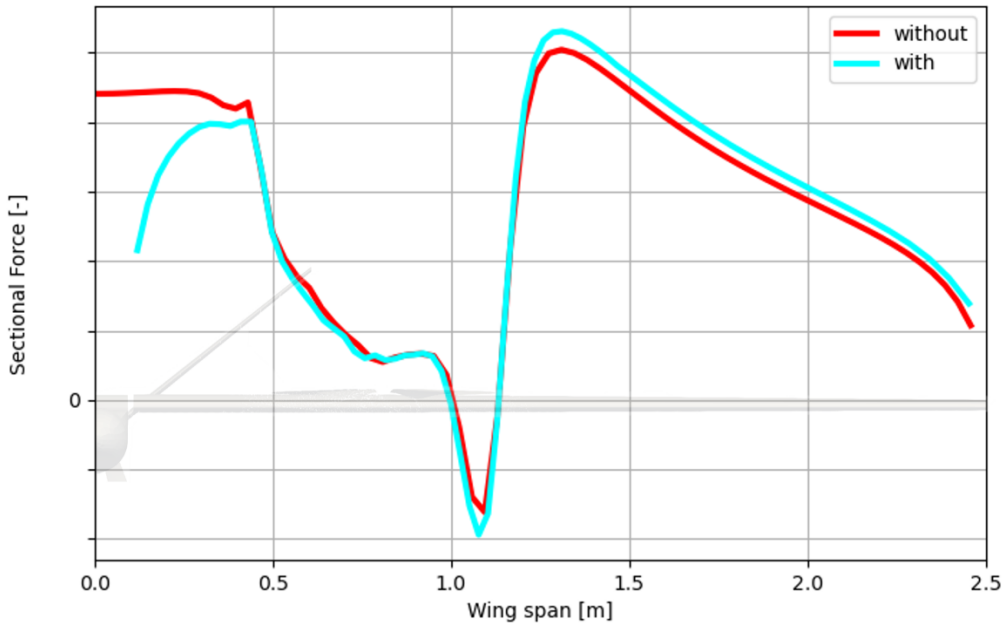

Figure 16: Load distribution over the wing in DUST with and without the presence of the fuselage.

Table 1: Forces comparison of DUST simulations between two different modelling approaches: with and without the fuselage.

CASE	FRONT PROPELLER THRUST	REAR PROPELLER THRUST	WING LIFT FORCE
% DIFFERENCE WITH/WO FUSELAGE	+0.1	-0.2	-7.03

As highlighted by Table 1, the difference for the front and rear propeller is minimal, whereas over the wing 7% less lift was produced in the case with the fuselage. Since the goal of the MF simulations is to introduce some physics-based trend to improve the predictions of a multi-fidelity ML application, it was decided to continue without the fuselage.

In addition, a comparison between the aerodynamic methods offered in DUST was performed at the same flight condition. Similar to the previous comparison, the relative thrust difference between the methods is negligible (see Table 2), whereas the main forces depend highly on the method chosen. Figure 17 do not show any important difference apart from some small irregular spikes present in the curves of LL and NL-VLM.

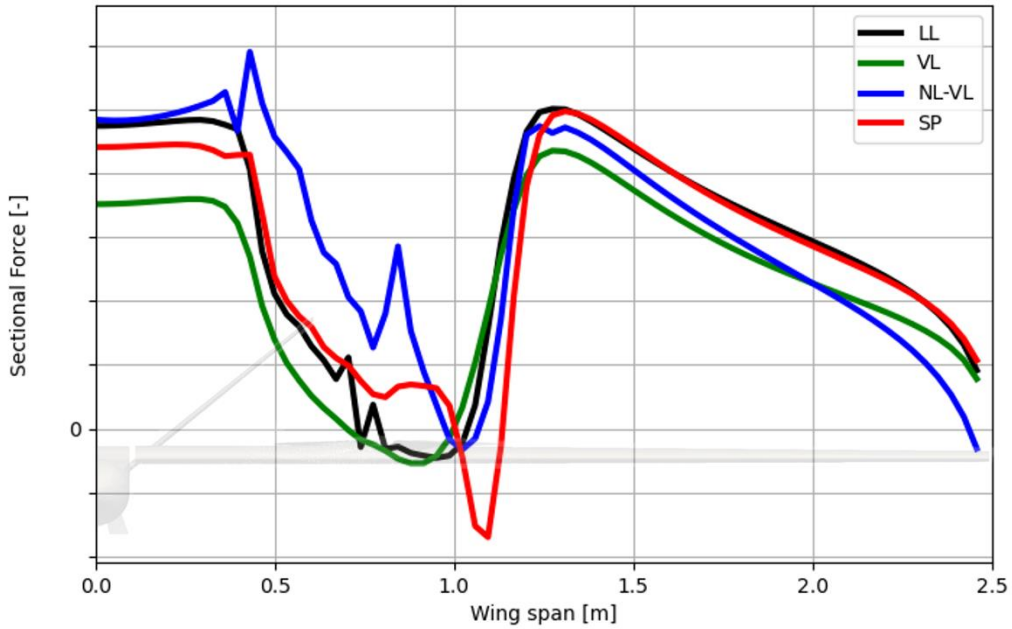

Figure 17: Load distribution over the wing comparison with methods: LL, VLM, NL-VLM and SP.

Table 2: Forces comparison of DUST simulations between different modelling of the wing aerodynamics. SP method taken as reference.

% DIFF BETWEEN METHODS	FRONT PROPELLER THRUST	REAR PROPELLER THRUST	WING LIFT FORCE
SP	-	-	-
NL-VL	+2.1	+0.3	+6.1
VL	-0.4	+3.0	-19.2
LL	+1.2	+7.0	+3.8

Another comparison in support of our methodology choice was performed by analysing the eVTOL aerodynamic forces without the influence of the propellers at high AOA. Calculations from 0° to 45° AOA were performed by

changing the aerodynamic method: LL, VLM, NL-VLM and SP were chosen. It is clear that VL and SP, being based on potential flow theory, do not show any stall-like effects. In fact, the C_L value continues to grow almost linearly. Whereas with NL-VLM and LL methods, leveraging the aerodynamic tables, the reduction in $C_L$and an increase in $C_D$is present. Despite being NL-VLM slightly computationally more expensive than LL, it was found to be more stable. Therefore for these reasons, it was decided as a method for our dataset calculation.

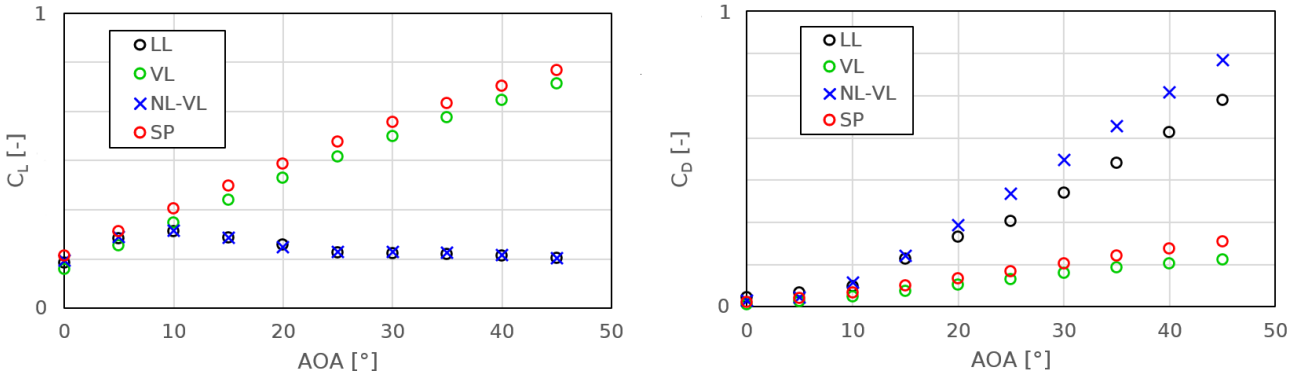

Figure 18: C_L and C_D over AOA in comparison with different methods (LL, VLM, NL-VLM and SP).

3.1.3 High-Fidelity

This section is about the results obtained on the HF CFD methods. Three different approaches are presented and analysed:

- Steady-state coarse grid CFD RANS (Airshaper automatic cloud-based solver)
- Steady-state mid grid CFD RANS (Airshaper automatic cloud-based solver)
- Transient fine grid CFD RANS (Ansys Fluent)

All cases were performed by using the same cleaned Skiron-X geometry and the same flow conditions. The study is conducted on a transition-like manoeuvre with all lift propeller rotational speed constant at the same value. In the first two cases, the Airshaper cloud-based application was used. The main reason was to test the cost-effectiveness of Airshaper approach, based on the automatization of all the main tasks. The solution is solved with steady-state RANS equations and k-omega SST turbulence model. The boundary layer is calculated by means of wall functions. The propellers are rotated thanks to multiple rotating domains. The first and second solutions differ only in the size of the grids, which are around 24 and 115 million cells.
The third case is a transient simulation performed with ANSYS Fluent. The calculation is also based on multiple reference frames for the propellers rotation and RANS equation with a realizable k-epsilon turbulence model. To track flow changes over time, a transient simulation was set-up. In addition and contrary to the two previous cases, here the boundary layer is fully resolved, meaning that the dimensionless wall length y+ is lower than one. To reduce the calculation computational costs, and since the simulation is symmetric with respect to the roll axis, only half model was simulated. After a sensitivity analysis study, the final mesh size was around 180 million cells. In addition, a DUST simulation is also compared with the other three HF cases.

As summarized in Table 3, both steady-state solutions exhibit a slightly larger propeller thrust compared to the transient CFD result, with a difference of less than 10%. This could be explained partly by the grid size and the temporal resolution. In comparison to the steady-state simulations, the transient case has a denser grid refinement around the propellers and their slipstream. Therefore, vorticity is better conserved and the propeller is subjected to a lower induced velocity, which results in a lower propeller thrust.

While DUST is considered an MF solver, vorticity is effectively conserved during its simulations, demonstrating its capability in handling rotational flows. In contrast, CFD simulations require finer grids to mitigate vorticity dissipation, especially in regions with complex vortical features. Due to the absence of experimental validation, it is challenging to definitively determine which is the most accurate solution. However, the relative difference between the front and back propeller thrust consistently falls within a 15-20% range across all simulations, suggesting a reasonable level of agreement.

The normal force coefficient C_Z^{WING} shows a notable discrepancy between the steady-state CFD cases and the DUST result, peaking a 29% difference with the steady-state coarse grid CFD case. The DUST solution yields a significantly higher coefficient, potentially attributable to the absence of the fuselage and the simplified approach used to model wing aerodynamics. While the VLM method offers computational efficiency and ease of use, it inherently neglects viscous effects and flow separation. Even with the inclusion of nonlinear corrections, the NL-VLM approach may still struggle to accurately capture separation phenomena.

It is important to note the significant disparity in human effort and computational resources required for MF and HF approaches. While implementing a DUST simulation is relatively straightforward, the Airshaper HF approach requires only a geometry preprocessing step. The effort involved increases further when adopting a standard approach by conducting transient simulations.

Table 3: Comparison of transition-like manoeuvre between HF and MF simulations.

METHOD	# OF ELEMENTS	FRONT PROPELLER THRUST [N]	REAR PROPELLER THRUST [N]	C_Z^{WING}
DUST	~1 M particles	22.72	19.5	0.373
STEADY CFD COARSE	~24 M cells	26.81	21.02	0.263
STEADY CFD MID	~115 M cells	27.63	22.13	0.267
TRANS CFD FINE	~180 M cells	24.9	17.8	0.282

Figures 19-21 illustrate the pressure distribution over the eVTOL wing for the three CFD simulations. The DUST top view differs from the other three due to its fundamentally different methodology and therefore is not reported. However, it effectively highlights the propeller-wing interaction, which is consistently observed in the same region across all CFD cases. In all HF cases, the propeller influence is readily apparent, with a more pronounced effect in the two steady-state simulations. The outboard wing section experiences an increase in pressure as the propeller decelerates the flow, whereas the inboard section exhibits a pressure decrease due to propeller-induced acceleration, resulting in a force decrease and increase, respectively. Moreover, the fuselage-wing interaction is remarkably consistent across all three cases.

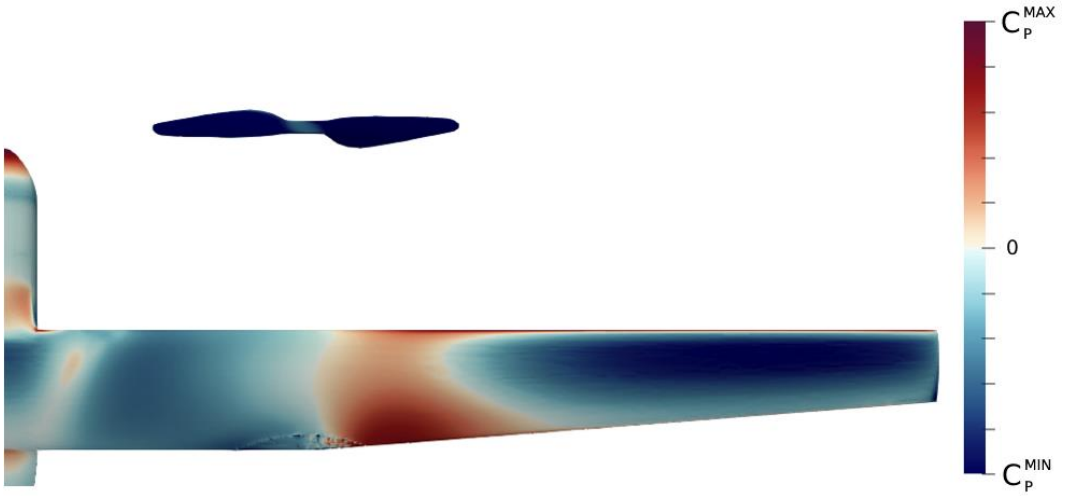

Figure 19: Wing pressure distribution during a transition-like manoeuvre of a HF steady-state coarse grid CFD simulation.

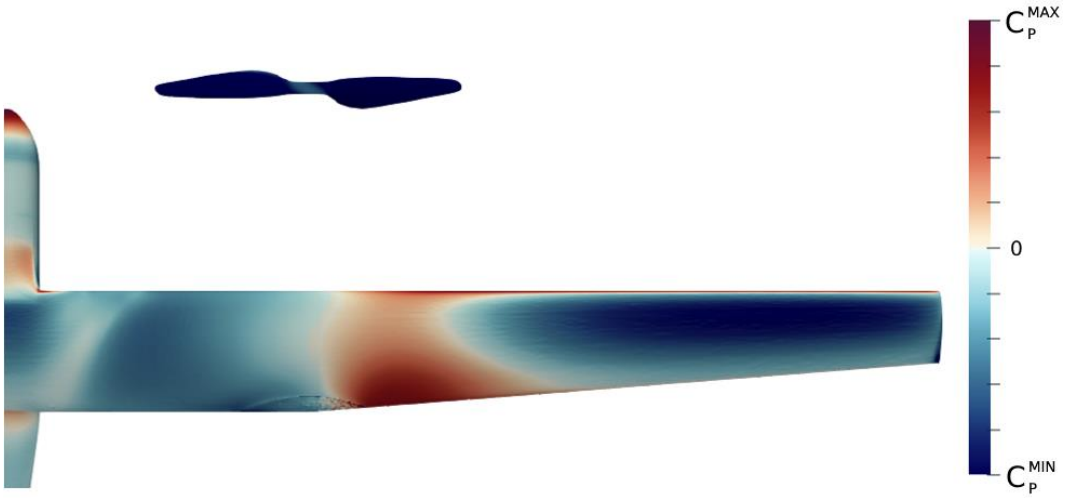

Figure 20: Wing pressure distribution during a transition-like manoeuvre of a HF steady-state fine grid CFD simulation.

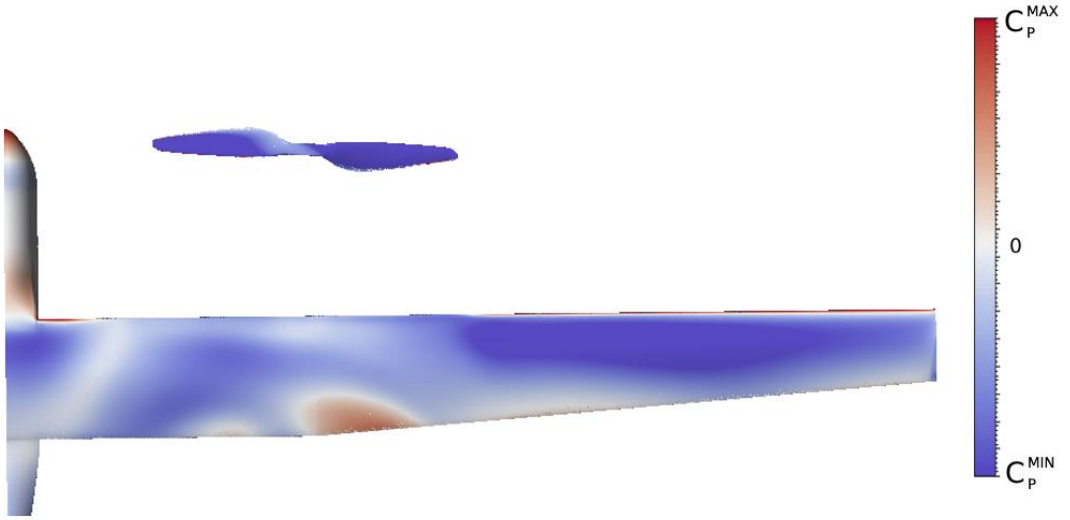

Figure 21: Wing pressure distribution during a transition-like manoeuvre of a HF transitional fine grid CFD simulation.

3.1.4 Aerodynamic comparison

Figure 22 shows the aerodynamic coefficient comparison of Skiron-X without the propellers between DUST (NL-VLM method) and CFD. The left and right figures show the lift and drag coefficient C_L and C_D over AOA, respectively. Despite the methods being quite different a good agreement has been found for both C_L and C_D.

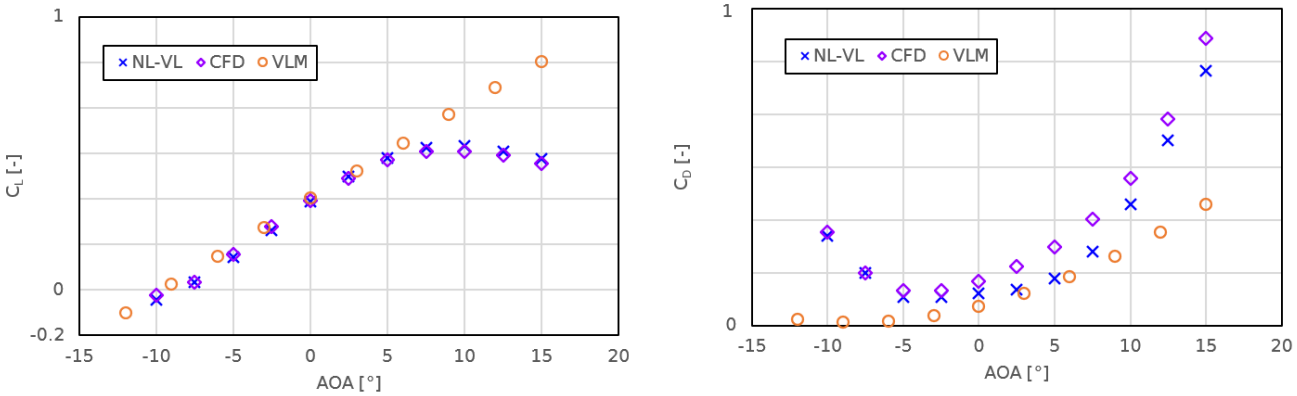

Figure 22: Aerodynamic coefficient comparison between DUST and CFD.

3.2 Multi-fidelity rotors data-driven model

This section provides the results of the multi-fidelity implementation of our model, from the dataset generation to the training and validation processes. The multi-fidelity model of Skiron-X is based on the comprehensive FSM described in section 2.1.1. An advantage of an LF FSM is usually the possibility to simulate the aircraft dynamics in real-time, being especially interesting for pilot-in-the-loop testing or to be used in a flight simulator. To leverage AI/ML systems, the FSM architecture remains the same and only some single parts are adapted. As depicted in Figure 23, the physics-based sub-modules replaced or improved by an AI/ML contribution are depicted in dark blue. In the Flight Mechanics Module, the Propulsion block of the Aircraft Module was completely replaced by the rotors data-driven model. Whereas in the Aeroelastic Module, both Steady and Unsteady Aerodynamic were improved by the ML-based model.
The process to build a BNN is not trivial and many iterations could be required to achieve a reasonable outcome. The first attempt was to improve the rotor prediction by fusing the data between LF and MF. It improves the prediction by accounting for the interaction between rotor-rotor and wing-rotor. The first step is to build the datasets from the two different fidelities. A simple BEM with inflow is used to generate the data in LF. The input points were chosen with the Latin Hypercube Sampling (LHS) method. This approach ensures a good spread of input data points across the entire propeller operating condition, leading to a more efficient and representative exploration of the parameter space in our simulations. Compared to random sampling, LHS often requires fewer data points to achieve a good representation of the input space. This leads to shorter simulation times and reduced computational costs.

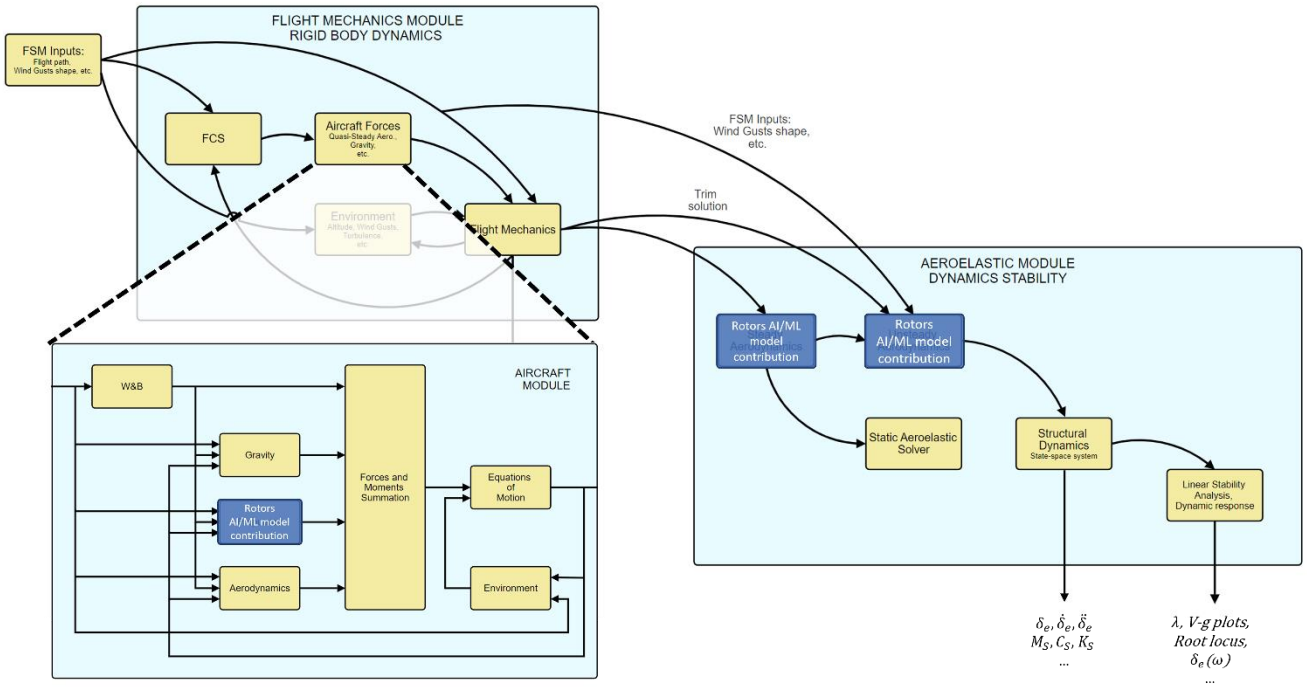

Figure 23: FSM architecture: Modules modified with the rotors AI/ML-based data-driven model are highlighted in blue.

On the other hand, the dataset with MF was generated by choosing the most representative points during HC, transition and AP mode. They represent roughly 10% of the entire dataset. Figure 24 shows the dataset of one propeller thrust over rotational speed and AOA, AOS and freestream velocity, respectively. Pink and green points are generated with LF and MF solvers, respectively.

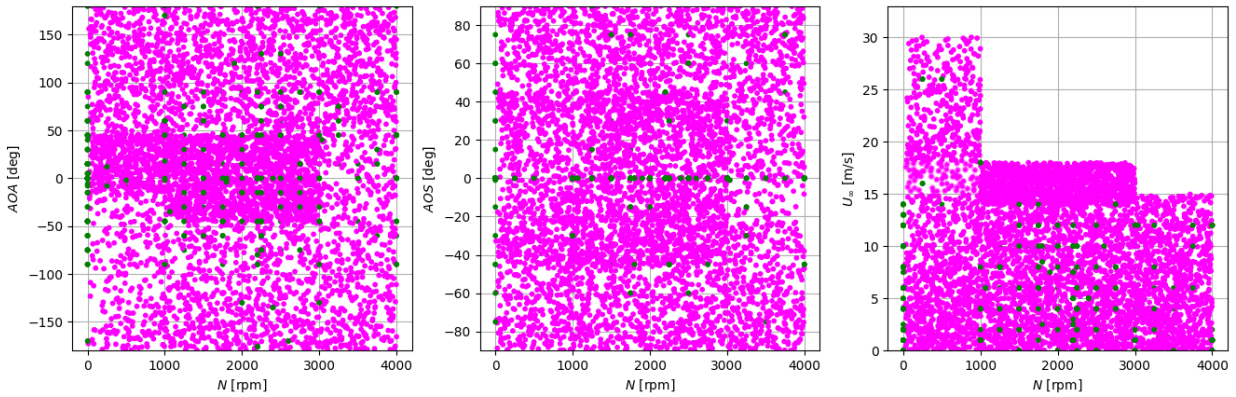

Figure 24: Propeller dataset for multi-fidelity implementation: LF and MF dataset are displayed in pink and green respectively.

Based on this data, the co-Kriging and BNN were trained as described in the previous section 2.6. The training phase starts with the training of the separated LF and MF datasets. Figure 25 and Figure 26 show the trend of train and validation loss during this process. The red segmented line represents the early stopping epoch.

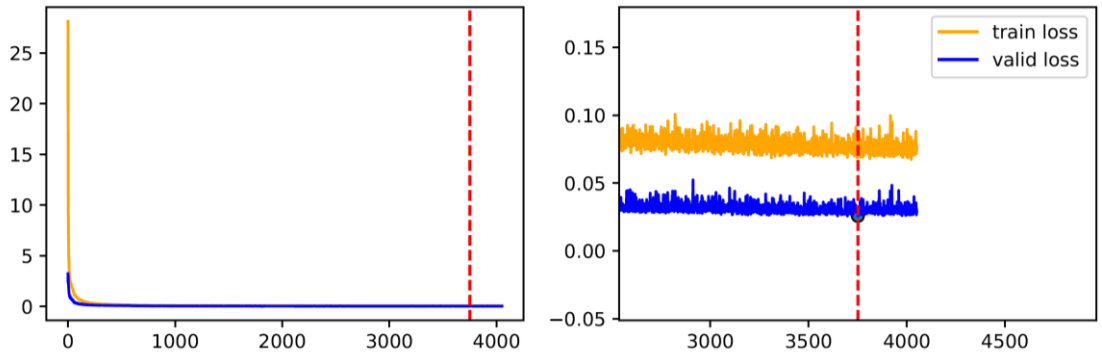

Figure 25: LF dataset BNN training history: training and validation loss curves are in orange and blue, respectively.

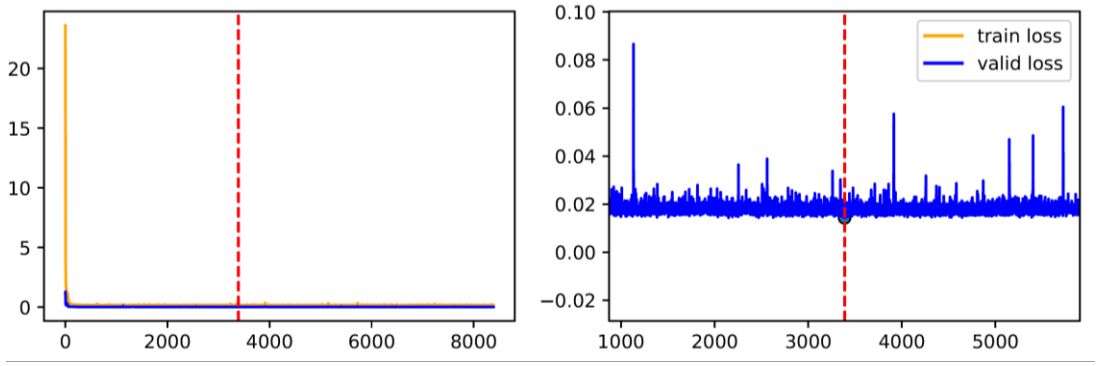

Figure 26: MF dataset BNN training history: training and validation loss curves are in orange and blue, respectively.

After this phase, the three last layers are then frozen, and subsequently the training is re-executed for the final tuning of the BNN. The trend of train and validation loss displayed on Figure 27.

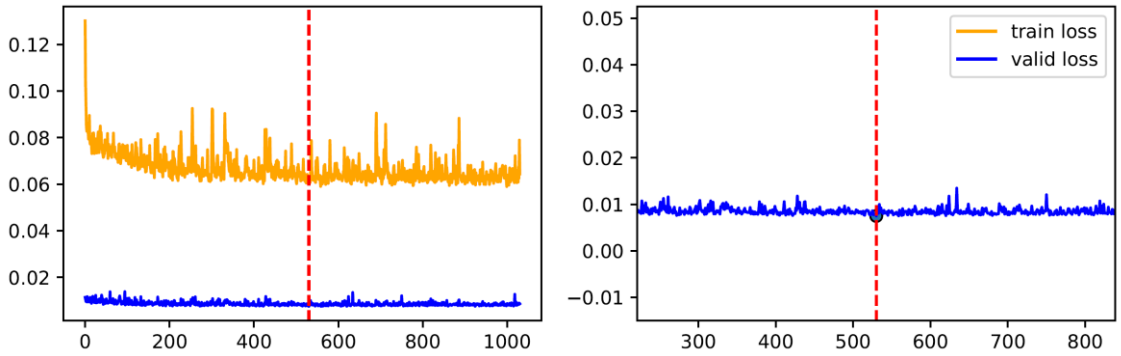

Figure 27: BNN training history after the Transfer Learning: training and validation loss curves are in orange and blue, respectively.

An example is shown in Figure 28 where the authors compare the performance of three BNN models (BNN-LF, BNN-MF, and BNN-TL) and Co-Kriging in predicting pusher propeller thrust at various revolution speeds and constant angle of attack and sideslip. BNN-LF, BNN-MF, and BNN-TL are trained on LF, MF, and with both LF and MF with transfer learning datasets, respectively.

While BNN-LF overestimates thrust and BNN-MF exhibits poor convergence due to limited data, BNN-TL demonstrates superior accuracy and reliability. It closely matches validation points and has a narrower confidence interval, indicating better prediction capability. This highlights the effectiveness of the data fusion approach using transfer learning in improving model performance. Similarly, the model based on Co-Kriging demonstrated also good results.

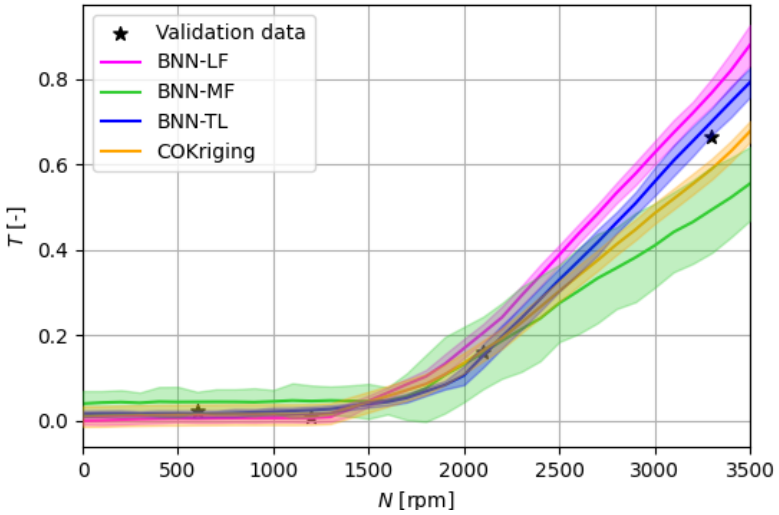

Figure 28: Thrust prediction over propeller rotational speed for LF, MF and the multi-fidelity BNN (orange, green and red).

Table 4 compares in detail the performance of the four ML models. The table includes average training time t_{train}, prediction time t_{pred} , total error ϵ_{tot}, and confidence interval σ_{tot}. Co-Kriging offers faster training and prediction speeds. However, BNN-TL demonstrates superior accuracy and reliability, as evidenced by its lower error and wider confidence intervals. This suggests that BNN-TL is better choice to capture the complexities of the system.

Table 4: Data-driven models comparison.

MODEL	t_{train} $[min]$	t_{pred} $[min]$	ϵ_{tot} [%]	σ_{tot} [%]
BNN-LF	41	0.020	4.88%	94.2
BNN-MF	35	0.020	10.8%	92.1
BNN-TL	55	0.020	3.06%	97.3
CO-KRIGING	4	0.005	3.9%	88.2

Representative points of the flight envelope predicted by the BNN model are subsequently reviewed by an expert of the field to determine if the model behavior is realistic and does not produce inconsistent values, especially for points that were not included in the training/validation set. This evaluation can also be done visually by examining the output curves of the model in each section of the input space.

Finally, we also analyzed in Figure 29 how the error on the test set changes as we progressively reduce the number of mid-fidelity samples. Data fusion reduced error values by approximately three times compared to the baseline. However, the uncertainty remained relatively stable, suggesting that the model has limited capacity to increase uncertainty for larger errors. This indicates that while data fusion improves accuracy, the model's uncertainty expression does not fully adjust to varying error levels when the training data is not enough. For this reason, it's crucial to have well-defined model hyperparameters and consistent data to achieve reliable predictions of both epistemic and aleatoric uncertainty. Proper tuning of hyperparameters ensures that the model captures the underlying data patterns effectively, while data consistency across fidelities helps the model better differentiate between predictable (aleatoric) and model-based (epistemic) uncertainties. Together, these elements enable a more accurate assessment of uncertainty, especially when training data is limited.

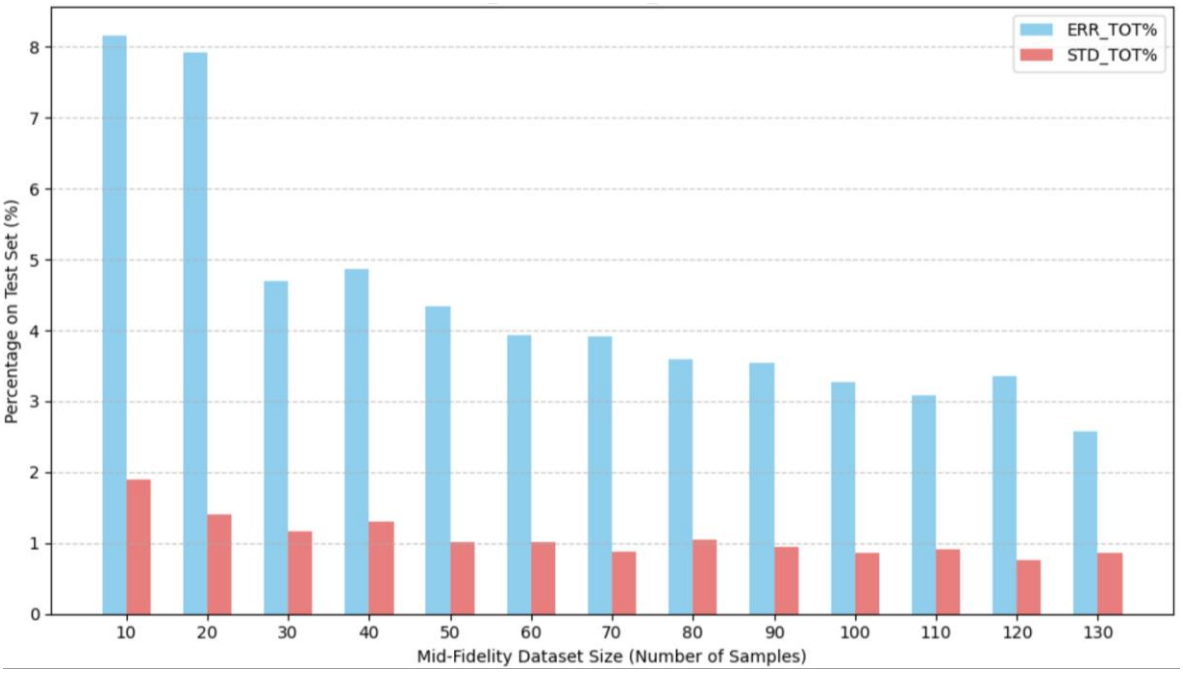

Figure 29: Variation of errors and std with reducing MF dataset size.

3.3 Flight Simulation Model evaluation

3.3.1 Flight Mechanics module comparison

Both physics-based Flight Mechanics module (see Figure 3) and its modified version improved by the AI/ML contribution (see Figure 23) are compared to the real aircraft trim conditions identified in the flight test data. These trim conditions consist of 8 to 20 seconds of straight and level flight, or full orbits of various diameters at constant airspeed and altitude. The mean values of the relevant flight test data parameters, such as airspeed, altitude and bank angle, were calculated. A trim algorithm was then used to trim the LF model in the same condition as the measured trim condition.

Figure 30 shows the performance of the LF model in comparison to the flight test data. From top to bottom, it depicts pusher propeller rotational speed, elevator deflection and wing root bending moment over True Air Speed (TAS). The flight test data of the wing root bending moment stem from the strain gauges installed on the vehicle. In general, the LF model captures the relevant characteristics of the aircraft. However, the model outputs do show biases relative to the flight test data. The similarity in trim elevator deflection and wing root bending moment across all airspeeds and trim conditions, both with and without the BNN-TL module, is notable. This consistency arises because the BNN-TL module influences only the propeller thrust and torque, leaving the aerodynamic and structural models almost unaffected. Notably, a limitation of the LF aerodynamic drag model is its tendency to underestimate the vehicle's parasitic drag.

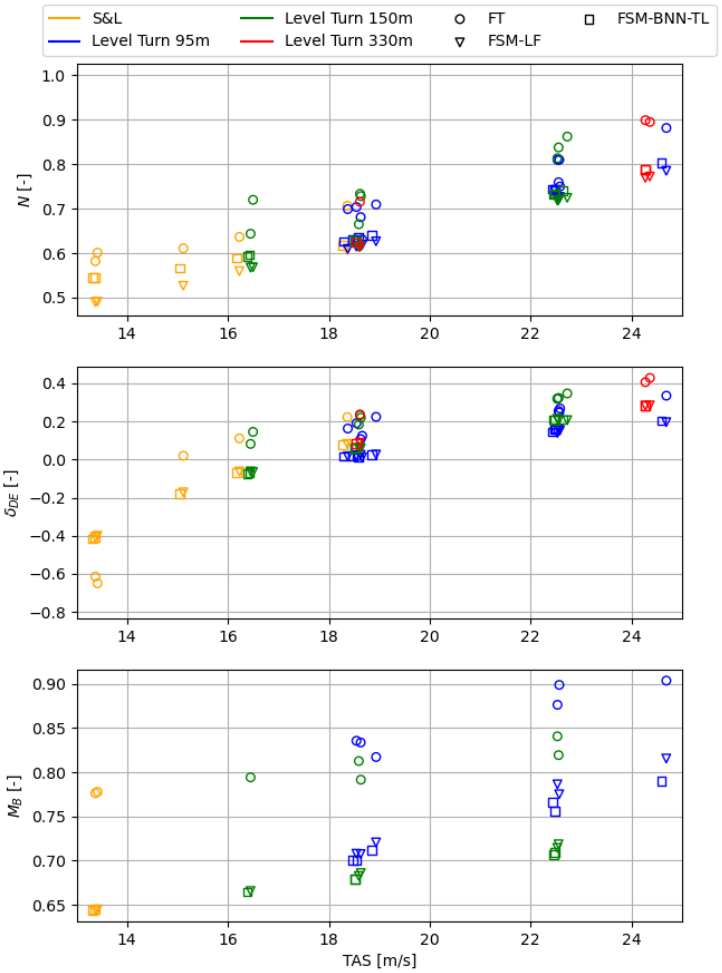

Figure 30: Comparison between flight test data (FT, circles)and both physics based FSM (FSM-LF, triangles) and AI/ML improved FSM (FSM-BNN-TL). Top image: pusher propeller rotational speed over TAS. Mid image: Elevator deflection over TAS. Bottom image: Wing Root Bending Moment over TAS.

3.3.2 Flight Mechanics module manoeuvres

In this section, several manoeuvres are analysed in HC and transition mode, while AP mode, being not as interesting as the others is omitted. The aerodynamics in HC to transition mode can be very complex, with rotor wake and wings downwash interacting with each other. On the other hand, in AP mode, the aerodynamics should be simpler and more solvable correctly with LF methods. All the following figures are a comparison of FSM-LF (dashed lines) and FSM-BNN-TL (solid lines) in different conditions. The four graphs show the timeseries of TAS, eVTOL aerodynamics lift L_{aero} and moment M_{aero}, propeller rotational speed N_{PP}, N_{FP} and N_{BP} (pusher, lift front and lift back propellers) and thrust T_{PP}, T_{FP} and T_{BP} (pusher, lift front and lift back propellers thrust). Since the manoeuvres are symmetrical with respect to the longitudinal axis, only front lift (red line) and back lift (green line) propellers data are shown, while the pusher propeller is displayed in blue.

The first case (see Figure 31) to be analysed is a forward flight in HC mode. Starting from a stable hovering condition, the eVTOL speed is increased up to a few m/s. Thanks to the top-right image, it is clear that a certain aerodynamic lift and a small nose-down moment are also generated from the wings, but is anyway not enough to sustain completely the eVTOL without the lift propellers. On the other hand, from the thrust plot (bottom-right), we can see that the curves from the FSM-LF and FSM-BNN-TL models overlap each other, in fact, the

dashed curves are barely visible. The most interesting finding comes from the rotational speed comparison (bottom-left). During hovering there is already a small difference between LF and BNN-TL predictions.

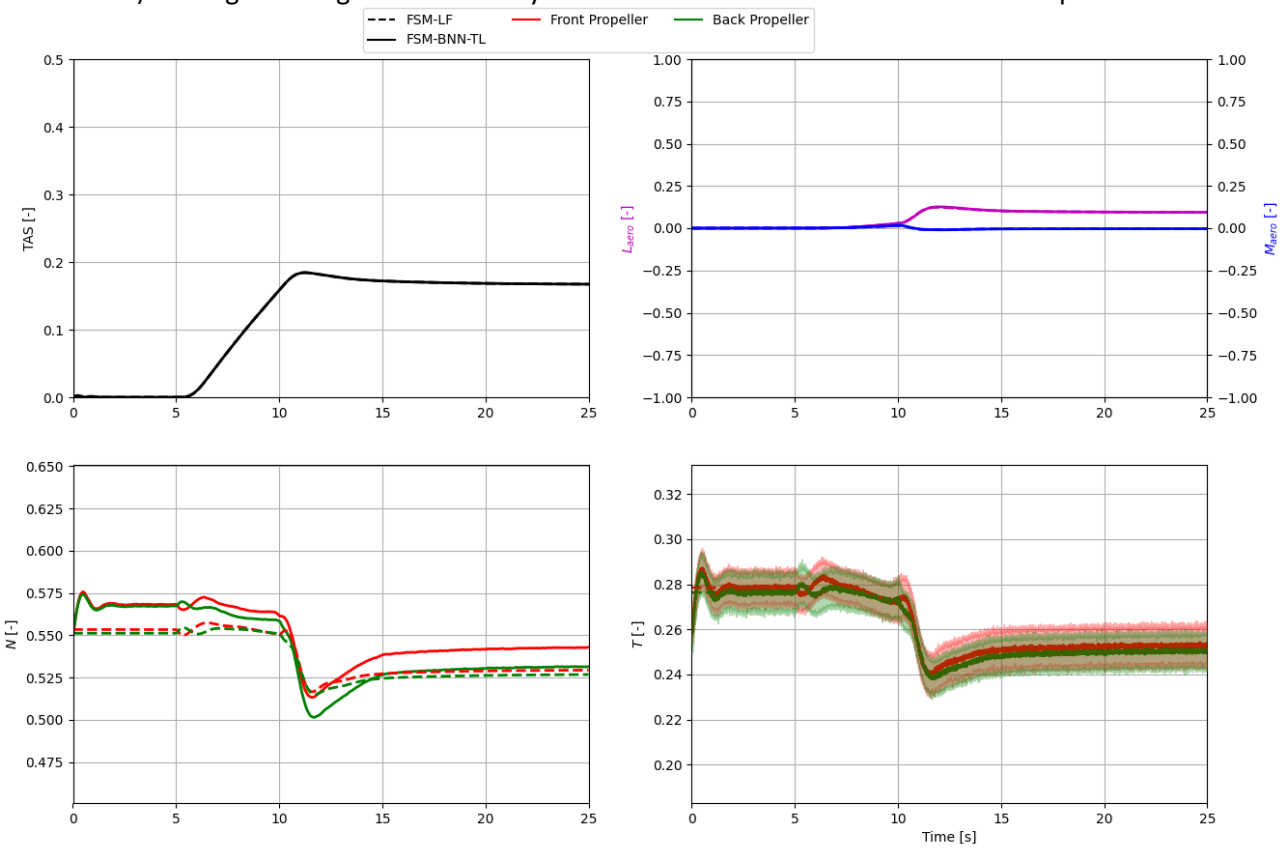

Figure 31: FSM forward flight in HC mode: TAS (top-left), eVTOL aerodynamics (top-right), propeller rotational speed N (bottom-left) and propeller thrust T (bottom right).

This could be attributed to a more realistic hovering data learned by the ML approach during the training. Furthermore, to achieve the same amount of thrust, more rotational speed is required from the FSM-BNN-ML. Thanks to the MF points, the interaction in this kind of situation, i.e. close to AOA=0° and a certain forward speed, is captured, while a standard LF inflow model is not able to model these effects.

The second case is depicted in Figure 32 and it describes a forward ascent in HC mode. Similar to the previous case, the eVTOl starts from a stable hovering condition, shortly after it starts to ascent for about 40 meters.
The top-right image confirms that the wings contribute to lift and moment, but contrary to the previous case, by ascending at a negative AOA, the eVTOL is generating a negative lift and a nose-up moment. The thrust plot (bottom-right) shows that the FSM-LF and FSM-BNN-TL models produce, as before, nearly identical results, with the dashed lines of FSM-LF being barely visible. However, the rotational speed comparison (bottom-left) reveals a slight difference between the LF and BNN-TL predictions during the manoeuvre. Similarly to the forward case, to generate the same thrust, the FSM-BNN-ML model requires higher rotational speeds compared to the FSM-LF model.

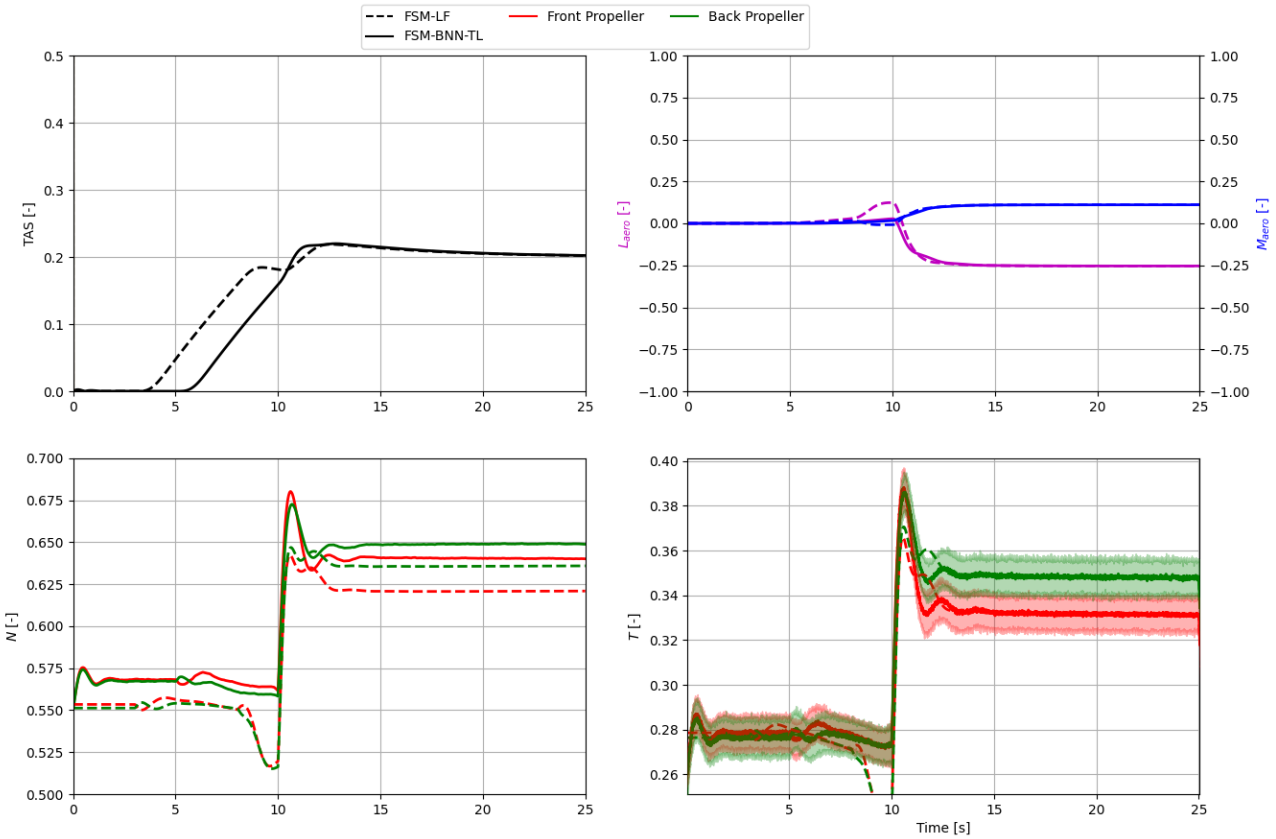

Figure 32: FSM forward ascent flight in HC mode: TAS (top-left), eVTOL aerodynamics (top-right), propeller rotational speed N (bottom-left) and propeller thrust T (bottom right).

The last HC case is shown in Figure 33 and describes a forward descent in HC mode. As in the previous cases, the eVTOL starts from a stable hovering condition, and shortly after it starts to fall for about 30 meters. The top-right plot shows that the wings are generating a certain lift and moment, but since the eVTOL is descending at a positive AOA, it generates a positive lift and a nose-down pitching moment. The thrust plot (bottom-right) shows that both FSM-LF and FSM-BNN-TL models produce nearly identical results, with FSM-LF lines being difficult to distinguish. As expected, the rotational speed comparison (bottom-left) reveals a certain difference between the FSM-LF and FSM-BNN-TL simulations. Similar to the forward flight case, the FSM-BNN-ML model requires higher rotational speeds to generate the same thrust compared to the FSM-LF model. In addition, here the gap between the solid red and green lines is lower than dashed lines, meaning that the difference between required rotational speed of lift front and back propeller of the ML approach is lower than LF method.

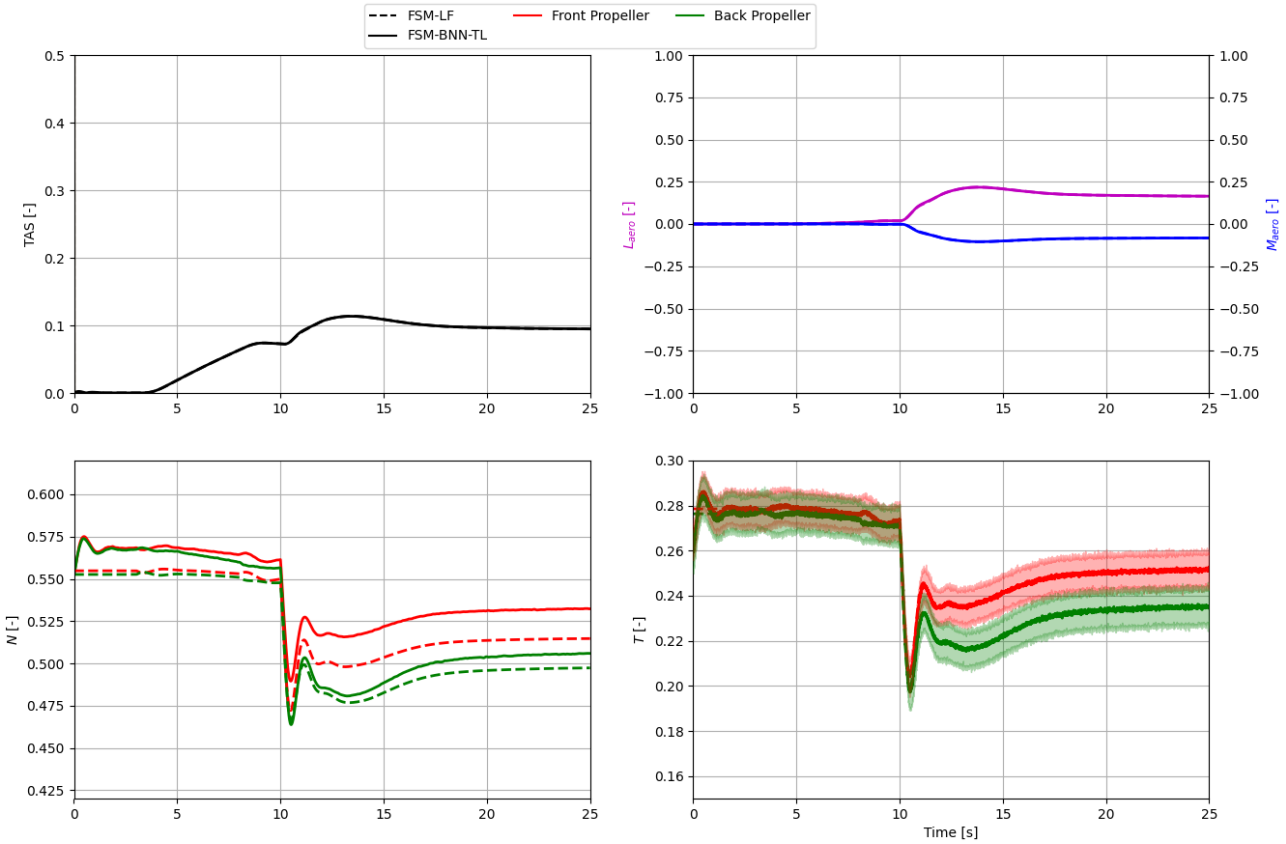

Figure 33: FSM forward descent flight in HC mode: TAS (top-left), eVTOL aerodynamics (top-right), propeller rotational speed N (bottom-left) and propeller thrust T (bottom right).

Figure 32 depicts a typical transition from hover control (HC) to autopilot (AP) mode. The top-left chart illustrates the eVTOL's true airspeed (TAS), which accelerates from 0 m/s in HC mode to a characteristic cruise speed in AP mode. The dashed and solid lines correspond to the FSM-LF and FSM-BNNTL results, respectively. This figure serves as a valuable indicator of the eVTOL's state during the transition phase. The top-right plot shows the lift and moment generated during the manoeuvre, where $L_{aero} > 1$ indicates that enough lift is generated by the wings to sustain a flight without lift propellers.

The bottom-left graph shows the rotational speeds of the pusher propeller (blue), left front (red), and back (green) propellers. Throughout this manoeuvre, the difference between the LF and BNN-TL pusher propeller speeds is minimal. A slight discrepancy arises only after the eVTOL reaches cruise speed, where the FSM-BNN-TL control system adjusts the pusher propeller trust to achieve a stable condition.

A more interesting comparison can be observed between the front and back lift propeller behaviour. The rotational speed difference is negligible in the LF case (dashed red and green lines). However, when using the BNN-TL model (solid red and green lines), a noticeable disparity emerges between the two propellers, with the difference increasing as airspeed rises. It is caused by the BNN-TL rotor model incorporation of the detrimental effects from the wake shedding. To compensate for the thrust reduction caused by the front rotor and wing wakes, the back propeller rotational speed needs to be higher than the front propeller.

The bottom-right figure, which displays the propeller thrust with confidence intervals, supports this observation. Between 12 and 20 seconds, the difference between N_{FP} and N_{BP} becomes significant, while the

predicted thrust T_{FP} and T_{BP} remain relatively similar. Another noteworthy finding from this graph is the increased standard deviation during the transition phase (approximately 3 to 20 seconds). This suggests that the BNN-TL model may exhibit reduced confidence in this region, prompting the FSM user to exercise greater caution in evaluating the results.

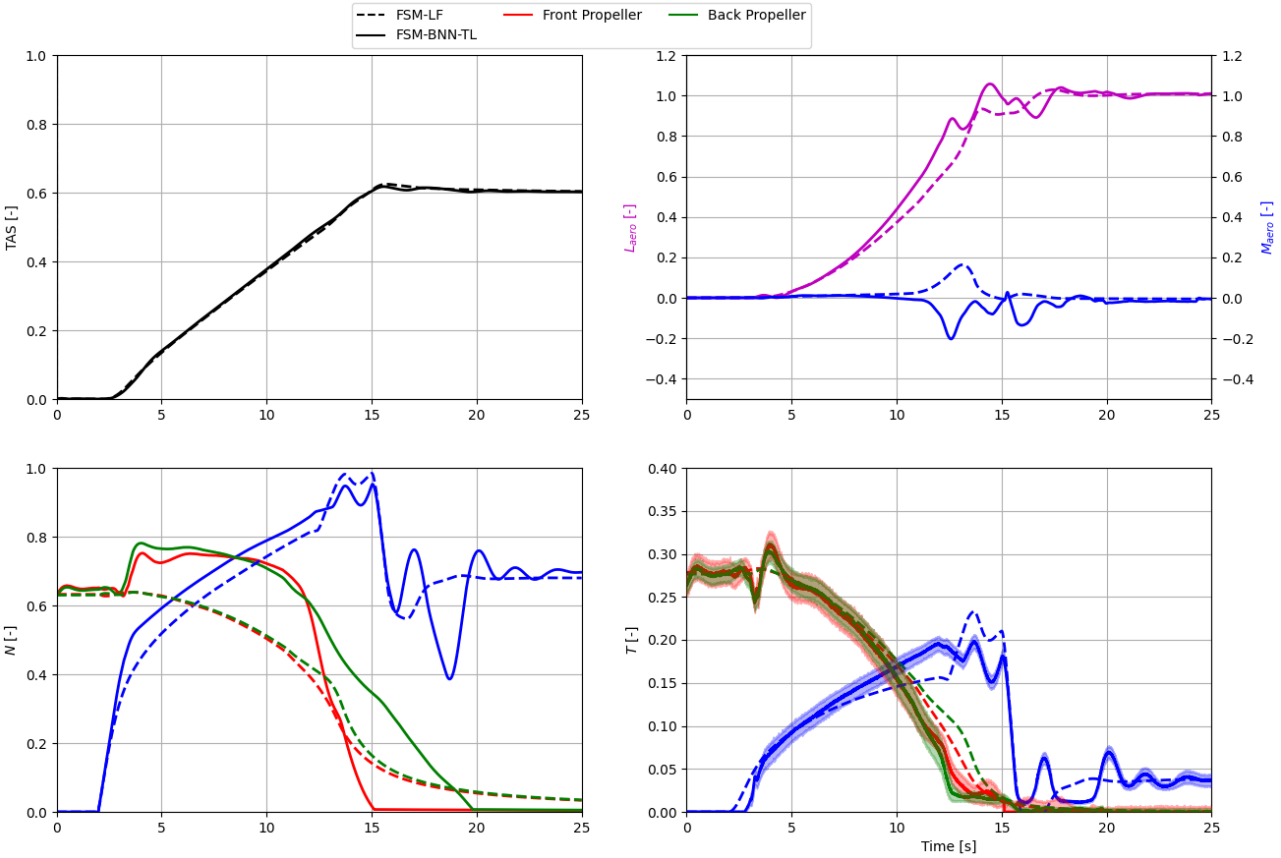

Figure 34: FSM transition from HC to AP mode: TAS (top-left), eVTOL aerodynamics (top-right), propeller rotational speed N (bottom-left) and propeller thrust T (bottom right).

Figure 35 depicts the same transition manoeuvre as the previous case but at a speed close to the maximum. The goal was to test the BNN-TL in a controlled condition outside its training space. The top-left curve approaches TAS =1.0, indicating that the eVTOL is nearing its maximum velocity. Compared to the previous case, the lift and moment plots exhibit more oscillations, likely due to the increased speed. The bottom graphs appear both those from the previous transition, except for the requirement for a higher pusher propeller rpm setting. Typically, N_{PP} should remain below 1.0, but the FCS is configured to allow temporary excursions above max if necessary. Since the BNN-TL model is not trained for operating conditions above 1.0, the bottom-left figure shows a widening of the confidence interval. This valuable information alerts the user that the simulation may not accurately represent real-world conditions or could potentially be erroneous in certain aspects.

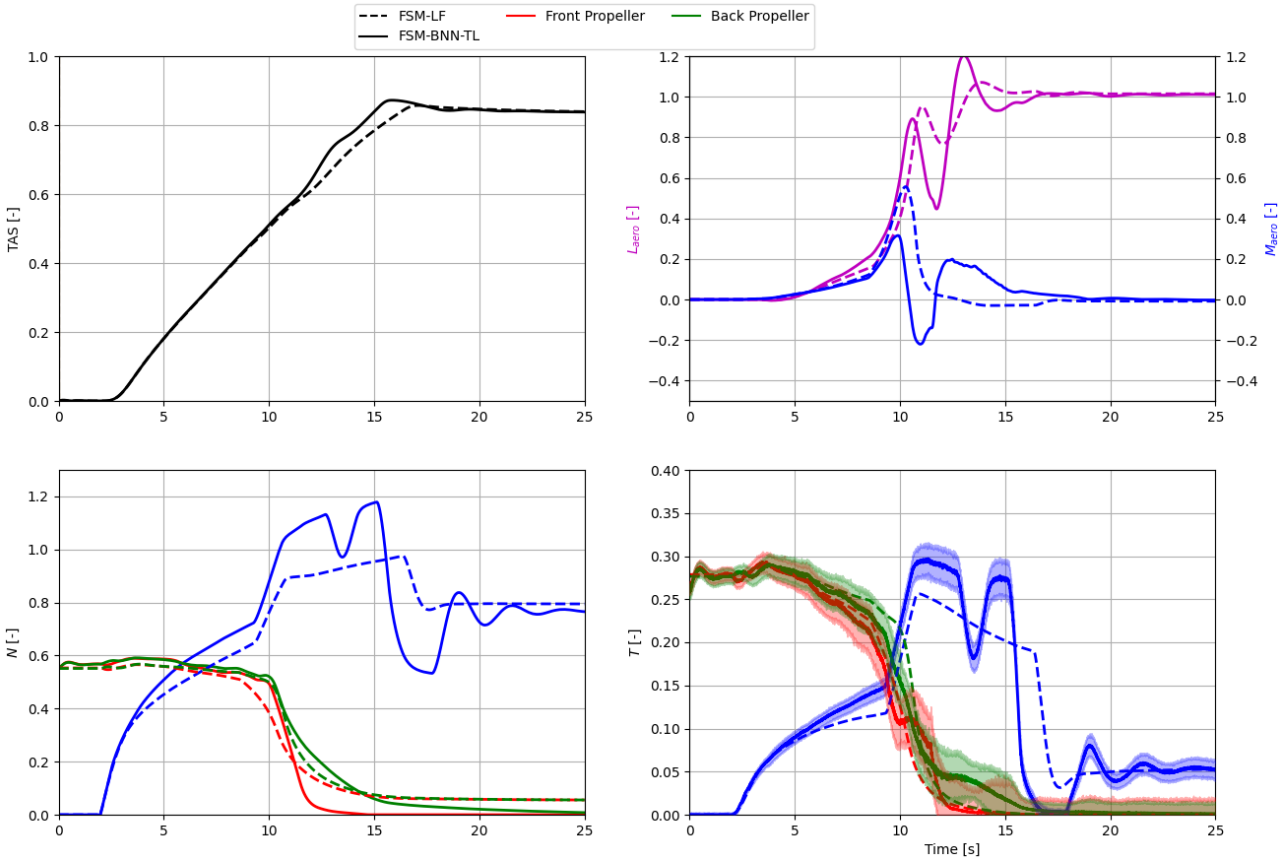

Figure 35: FSM transition from HC to AP mode at max speed: TAS (top-left), eVTOL aerodynamics (top-right), propeller rotational speed N (bottom-left) and propeller thrust T (bottom right).

3.3.3 Aeroelastic module

As described in Figure 5 and Figure 7, the Aeroelastic module integrates both elastic and rigid degrees of freedom from a FEM of the aircraft. The FEM is constructed using beam elements and calibrated to match the modal frequencies and natural frequencies obtained from a ground vibration test. Aerodynamic forces are modelled using a state-space approach similar to that described by Leishman and Nguyen [19], while the steady rotor thrust values are derived from the Flight Mechanics module. This integrated model enables time-domain analysis of nonlinear dynamic response and can be linearized for assessing linear stability and dynamic response in the frequency domain.

Figure 36 compares the wing root mean square (RMS) values of wing bending moments (left) and CG accelerations (right), as predicted by a reduced-order model and experimental data, across different flight points (FP). These experimental points are taken and averaged from several “level turns” manoeuvres at different radius sizes between 100 and 200 meters. Discrete gusts of varying magnitudes, calibrated to match both bending moments and accelerations, were used as perturbations. The blue line represents model predictions, while the black line with star markers denotes experimental results. The shaded area within the radar plot highlights regions of higher RMS bending moments, identifying critical points for structural integrity assessment under turbulent and gusty conditions. This plot visually demonstrates the model accuracy in replicating real-world scenarios, validating its reliability.

Figure 37 presents V-g plots that illustrate the system aeroelastic stability and frequency response in HC (left) and AP (right) modes. The top subplot shows the variation of damping ratio ξ/ω_{ref} with respect to normalized

velocity U/U_{ref}. This subplot is crucial for identifying critical speeds where system damping approaches zero, indicating the onset of flutter or other instabilities. The bottom subplot shows the variation of frequency f/f_ref with respect to normalized velocity U/U_{ref}. This plot highlights variations in model frequencies, including potential coalescence of different modal frequencies at higher velocities, which can also indicate instability regions.

Figure 38 presents root locus plots in HC and AP modes, respectively, offering the same information as the previous image but in a format (imaginary part versus the real part of the eigenvalues) that more readily highlights the mechanisms underlying unstable modes. Overall, the aeroelastic analysis did not identify any instabilities or unexpected behaviours.

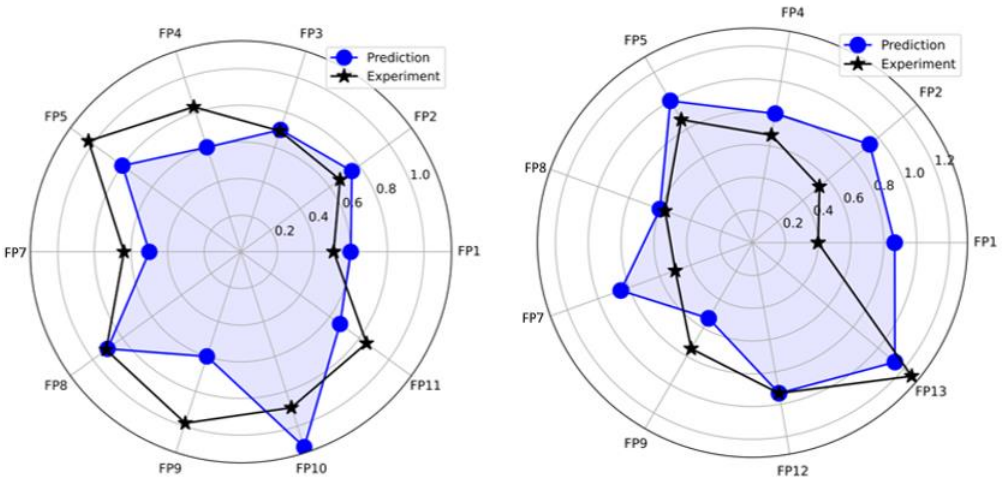

Figure 36: Wing bending (left) and CG (right) acceleration RMS.

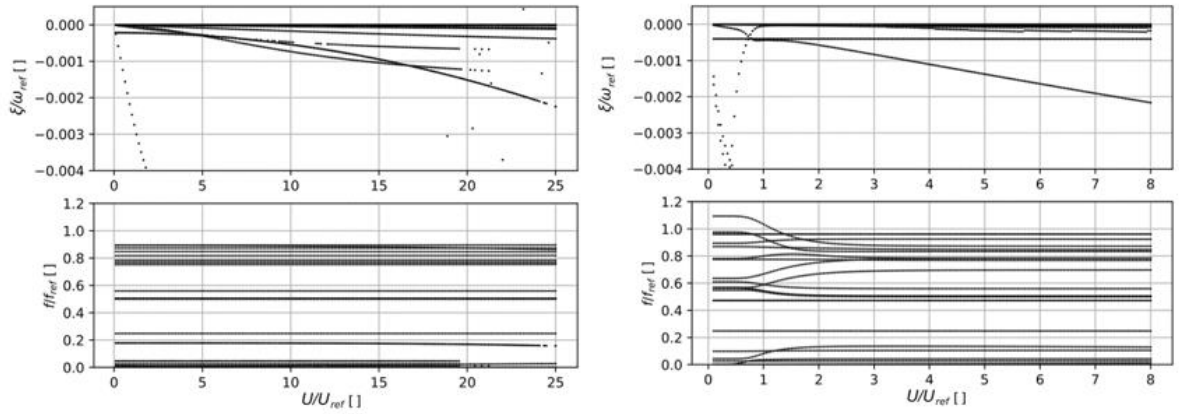

Figure 37: V-g plots in HC (left) and AP mode (right).

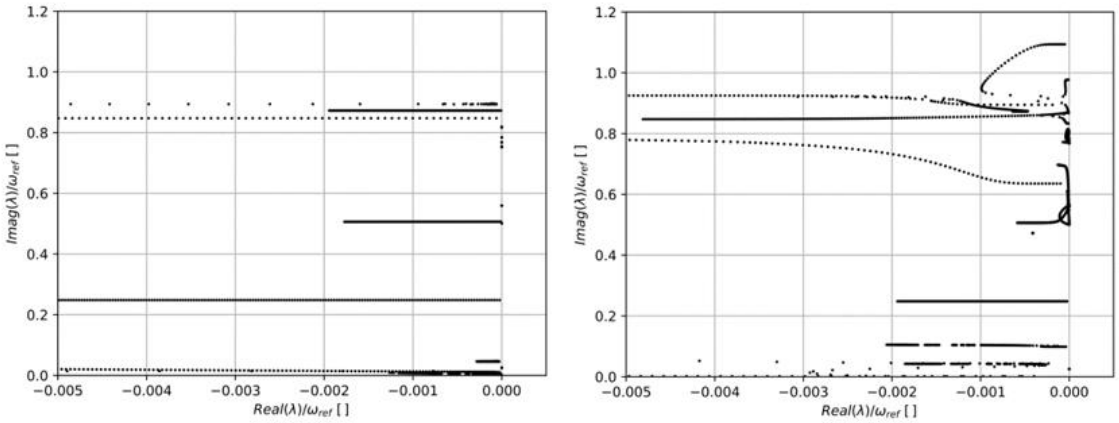

Figure 38: Root locus in HC (left) and AP mode (right).

4. Conclusions

Thanks to this case study, the authors explored and developed several physics-based and data-driven models of the eVTOL Skiron-X from Aurora Flight Sciences. The final model is a FSM capable of performing a wide range of static and dynamic analyses, including aircraft trim for steady flight conditions, the simulation of the critical transition phase between HC and AP modes, and the aeroelastic analyses (dynamic response, dynamic stability assessment).

The FSM is constructed using a modular approach and consists of a Flight Mechanics and an Aeroelastic module. Each sub-module is initially developed as a physics based LF model focusing on a single field, such as steady aerodynamics. This modular architecture facilitates modifications and improvements to individual modules without affecting the overall system. For instance, one could enhance the fidelity of the steady aerodynamics while maintaining a LF representation of the structure. Furthermore, and more notably within the context of this project, the modular approach enables the replacement of one or more modules with data-driven models. The key point of our approach is the handling of the complexity of the vehicle's aerodynamics through data-driven multi-fidelity techniques. The accuracy and robustness of this approach are enhanced by the application of ML methods, which also provide an indication of the model uncertainties. We emphasize that ML is not strictly necessary for our approach to work. However, ML is much more powerful than conventional approaches.

The structural model of Skiron-X was successfully reduced and validated using flight test data. Eigenfrequencies extracted from strain gauges and accelerometers data were used to fine-tune the wing profiles and ensure accurate simulation of dynamic characteristics. FFT analysis of strain gauge data identified key eigenfrequencies associated with bending and torsional modes, supporting structural assessment and model validation.

Aerodynamic modeling was a focal point of this research. LF models, widely used in the aerospace industry, include methods like VLM and strip theory. On the other hand, MF methods, more specifically VPM, have been developed substantially and seen their popularity rise steadily over the past few years. They are based on a Lagrangian description of the Navier-Stokes equations in their velocity-vorticity form and therefore prone to conserve complex vortical structures.
The DUST code, the software suite we have been using, underwent extensive testing with various benchmark cases. Skiron-X was modeled using different approaches to identify the most suitable method for our case study. The four available aerodynamic methods, LL, VLM, NL-VLM, and SP, were analyzed. While in the absence of separation, SP is generally considered the most accurate, NL-VLM demonstrated superior robustness and physical representation for our purposes. NL-VLM was used for propellers, wings, and tails to calculate aerodynamic forces with a time-step resolution for each 5° azimuthal blade angle rotation. Comparisons with LF VLM and CFD revealed strong agreement with DUST, especially post-stall. The DUST code was employed to generate the dataset for the data-driven model of the five propellers.

At the beginning of the project, CFD was selected as the HF method. However, after an initial investigation focused on modeling propellers using an embedded actuator disk model within the CFD domain, it became immediately clear that the actuator disk is no suitable approach for eVTOL aircraft as its tuning requires a significant effort. We then investigated the use of CFD with different approaches, namely modelling propellers as separate rotating domains with the multiple reference frame technique surrounded by the static fluid domain, which contains the aircraft body and wings. A key challenge of this approach is the dissipation of vorticity, which can prevent capturing rotor-wing-tail interactions suitably. To address this issue, a fine grid of the wake is required, leading to a large number of cells and substantial computational costs. To mitigate human

effort, an automated approach proposed by Airshaper was also tested in addition to the traditional method. Findings from this task indicate that reliable results necessitate unsteady and large-grid size CFD models, which may be impractical for certain applications due to time and resource constraints. The authors suggest that such CFD is a valuable approach which can only be trusted with eVTOL flows if spatial and temporal resolution are sufficiently high and as such is a very expensive one to exploit for validation purposes only.

After the dataset generation phase, a data-driven model for all rotors was implemented and tested with both Co-Kriging and BNN-TL techniques. While Co-Kriging offers a simpler and faster implementation with an average training time approximately one order of magnitude lower than the BNN approach, BNN-TL demonstrated superior prediction capabilities with an average error of $\epsilon = 1.8\%$. We point out again, that although ML is not strictly necessary for this approach, it significantly improves the system's ability to handle realistic scenarios. This is confirmed by the results presented in Chapter 3.

Firstly, the FSM is compared to flight test data collected with Skiron-X. Both FSM models, with and without integrated BNN-TL propeller models, were analysed. In general, both models exhibit a similar trend to FT data. Finally, demonstrates the improvement achieved by integrating the ML component into the FSM. During a transition from HC to AP mode, the FSM with the integrated BNN-TL propeller thrust model exhibited more realistic behaviour. The back propeller thrust reduces with respect to airspeed due to the front propeller and wing wakes, which create a non-ideal perturbed inflow condition.
A good indicator of the simulation uncertainty is given by the confidence interval. In the first four manoeuvres presented, no particular anomalies are observed, while in the last case, where the data-driven model is forced to extrapolate a prediction, a higher standard deviation is reported (see Figure 35), which would make the user aware of the possible low reliability of the model outcome.

The aeroelastic model, incorporating both elastic and rigid degrees of freedom, accurately predicts the dynamic response of the aircraft under various flight conditions. The model's ability to replicate real-world scenarios, as demonstrated by the comparison of RMS values and V-g plots, validates its reliability for assessing system stability and frequency response. The root locus analysis further confirms the absence of any identified instabilities, providing confidence in the structural integrity of the aircraft. While our model pertains to a 22 kg drone, the complexity of the physics involved is comparable to that of larger eVTOL aircraft.

In general, we find our results encouraging and believe that the proposed modular approach and the multi-fidelity method not only reduce the computational costs associated with static and dynamic modelling of eVTOL aircraft but they can achieve a level of accuracy suitable to be exploited for certification purposes. Additional AI/ML algorithms may be further exploited in this endeavour by including parametric regression models to keep the rotor dynamics into account.

Bibliography

[1] Andrea Pedrioli, Marcello Righi. MODEL-SI, D-1.1 Report literature and digital solutions review. Research Project EASA.2022.C25, 2023.

[2] Manuel Reyes, Hector Climent, Moti Karpel, Felix Ar´evalo, and Carlos Maderuelo. Examples on increased order aeroservoelastic modeling. In *CEAS Aeronautical Journal*, 10:1071–1087, 2019.

[3] Moti Karpel, Alexander Shousterman, Carlos Maderuelo, and H´ector Climent. Dynamic aeroservoelastic response with nonlinear structural elements. In *AIAA Journal*, 53(11):3233–
3239, 2015.

[4] Wayne Johnson. *Rotorcraft Aeromechanics*. Cambridge University Press, 1 edition, April 2013.

[5] Björn Montgomerie. Methods for Root Effects, Tip Effects and Extending the Angle of Attack Range to ±180°, with Application to Aerodynamics for Blades on Wind Turbines and Propellers. Scientific Report, Swedish Defence Research Agency, ISSN 1650-1942, 2004.

[6] Larry A. Viterna, David C. Janetzke. Theoretical and Experimental Power From Large Horizontal-Axis Wind Turbines. NASA Technical Report No. DOE/NASA/20320-41, 1982.

[7] USDOD, “Flying qualities of piloted aircraft. Mil. Stand. MIL-STD-1797A (Notice 3),” 2004.

[8] Andrea Zanotti, Alberto Savino, Michele Palazzi, Matteo Tugnoli, and Vincenzo Muscarello. Assessment of a Mid-Fidelity Numerical Approach for the Investigation of Tiltrotor Aerodynamics. In *Applied Sciences*, 11(8):3385, 2021.

[9] Edoardo J. Alvarez. Reformulated Vortex Particle Method and Meshless Large Eddy Simulation of Multirotor Aircraft. Brigham Young University Ph.D. Thesis, 2022.

[10] “Airshaper webpage”, 2024. https://airshaper.com/, last access: 11.10.2024.

[11] “Ansys Fluids webpage”, 2024. https://www.ansys.com/products/fluids, last access: 11.10.2024.

[12] Wouter Remmerie and Nikola Majksner. Open source tools for OpenFOAM - Adaptive mesh refinement and convergence detection. In *IOP Conf. Series: Materials Science and Engineering* 1312 (2024) 012013, 2024.

[13] Andrea Vaiuso, Gabriele Immordino, Marcello Righi, Andrea Da Ronch. Multi–Fidelity Bayesian Neural Network for Uncertainty Quantification in Transonic Aerodynamic Loads. In *ArXiv* 2407.05684, 2024.

[14] Bruno Sudret. Global sensitivity analysis using polynomial chaos expansions. In *Reliability engineering & System Safety* 93(7):964-979, 2008.

[15] Bret Stanford, and Massey J. Steven. Uncertainty Quantification of the Fun3d-Predicted Nasa Crm Flutter Boundary. In *AIAA SciTech 2017 Forum*, Grapevine, TE, Jan 2017.

[16] Marcello Righi, Carnevali Lapo, and Marco Ravasi. Uncertainties Quantification in Flutter Prediction of a Wind Tunnel Model Exhibiting Large Displacements. In *AIAA SciTech 2022 Forum*, San Diego, CA, Jan 2022.

[17] "XFoil offical webpage", 2024. https://web.mit.edu/drela/Public/web/xfoil/, last access: 04.06.2024.
[18] "QBlade official webpage", 2024. https://qblade.org/, last access: 04.06.2024.
[19] Jay Gordon Leishman and Khiem Nguyen. State-space representation of unsteady airfoil behavior. In *AIAA Journal* Vol. 28 No. 5, 1990

European Union Aviation Safety Agency

Konrad-Adenauer-Ufer 3
50668 Cologne
Germany

Mail EASA.research@easa.europa.eu
Web www.easa.europa.eu

An Agency of the European Union